

ORIGINAL ARTICLE OPEN ACCESS

Concurrent Measurement of O₂ Production and Isoprene Emission During Photosynthesis: Pros, Cons and Metabolic Implications of Responses to Light, CO₂ and Temperature

Kolby Jeremiah Jardine¹  | Suman Som¹ | Luiza Beraldi Gallo^{1,2} | Jilian Demus³ | Tomas Ferreira Domingues²  | Christina Marie Wistrom³ | Lianhong Gu⁴  | Guillaume Tcherkez^{5,6}  | Ülo Niinemets⁷ 

¹Lawrence Berkeley National Laboratory, Climate and Ecosystem Sciences Division, Berkeley, California, USA | ²FFCLRP, Departamento de Biologia, Ribeirão Preto, University of São Paulo, São Paulo, Brazil | ³College of Natural Resources, University of California, Berkeley, Berkeley, California, USA | ⁴Oak Ridge National Laboratory, Environmental Sciences Division and Climate Change Science Institute, Oak Ridge, Tennessee, USA | ⁵Division of Plant Sciences, Research School of Biology, Australian National University, Canberra, Australian Capital Territory, Australia | ⁶Institut de Recherche en Horticulture et Semences, INRAE, Université d'Angers, Beaucouzé, France | ⁷Chair of Plant Biology and Crop Science, Estonian University of Life Sciences, Tartu, Estonia

Correspondence: Kolby Jeremiah Jardine (kjjardine@lbl.gov)

Received: 24 October 2023 | **Revised:** 13 August 2024 | **Accepted:** 17 August 2024

Funding: This study was supported by US Department of Energy (DOE), Office of Science, Office of Biological and Environmental Research (BER), Biological System Science Division (BSSD), Early Career Research Programme (Grant FP00007421), Lawrence Berkeley National Laboratory, and the Next-Generation Ecosystem Experiments-Tropics (NGEE-Tropics), (Grant DE-AC02-05CH11231).

Keywords: electron transport | gross oxygen production | H₂¹⁸O labelling | isoprene | isotope labelling | lipid metabolism | net oxygen production | photorespiration | photosynthesis | thermotolerance

ABSTRACT

Traditional leaf gas exchange experiments have focused on net CO₂ exchange (A_{net}). Here, using California poplar (*Populus trichocarpa*), we coupled measurements of net oxygen production (NOP), isoprene emissions and $\delta^{18}\text{O}$ in O₂ to traditional CO₂/H₂O gas exchange with chlorophyll fluorescence, and measured light, CO₂ and temperature response curves. This allowed us to obtain a comprehensive picture of the photosynthetic redox budget including electron transport rate (ETR) and estimates of the mean assimilatory quotient ($\text{AQ} = A_{\text{net}}/\text{NOP}$). We found that A_{net} and NOP were linearly correlated across environmental gradients with similar observed AQ values during light (1.25 ± 0.05) and CO₂ responses (1.23 ± 0.07). In contrast, AQ was suppressed during leaf temperature responses in the light (0.87 ± 0.28), potentially due to the acceleration of alternative ETR sinks like lipid synthesis. A_{net} and NOP had an optimum temperature (T_{opt}) of 31°C, while ETR and $\delta^{18}\text{O}$ in O₂ (35°C) and isoprene emissions (39°C) had distinctly higher T_{opt} . The results confirm a tight connection between water oxidation and ETR and support a view of light-dependent lipid synthesis primarily driven by photosynthetic ATP/NADPH not consumed by the Calvin–Benson cycle, as an important thermotolerance mechanism linked with high rates of (photo)respiration and CO₂/O₂ recycling.

1 | Introduction

Terrestrial ecosystems cycle large amounts of carbon dioxide (CO₂) and oxygen (O₂) between the biosphere and atmosphere

via photosynthesis, photorespiration and respiration. However, the majority of gas exchange observations of photosynthesis and (photo)respiration from individual leaves under controlled environmental conditions have focused on biological and

This is an open access article under the terms of the [Creative Commons Attribution-NonCommercial-NoDerivs](https://creativecommons.org/licenses/by-nc-nd/4.0/) License, which permits use and distribution in any medium, provided the original work is properly cited, the use is non-commercial and no modifications or adaptations are made.

© 2024 The Author(s). *Plant, Cell & Environment* published by John Wiley & Sons Ltd.

environmental variables impacting net CO₂ assimilation (A_{net}) without the inclusion of gaseous products of photosynthesis such as O₂ and isoprene emissions. The lack of leaf-atmosphere O₂ flux data is largely due to the technical difficulty of measuring a small change in O₂ mole fraction (e.g., 2–200 ppm O₂) in a high atmospheric O₂ background (21%, i.e., 210 000 ppm), that is, the high measurement precision needed to clearly resolve relatively small atmospheric O₂ concentration changes in gas-exchange systems (Kim-Hak et al. 2018). The experimental challenge has been partly solved by O₂ measurements under low ambient O₂ concentrations (1%–2%) (Laisk et al. 2002). However, low O₂ concentration itself has impacts on leaf gas exchange, suppressing photorespiration and potentially ‘mitochondrial’ respiration (also referred to as day respiration), but often also inducing feedback-limited photosynthesis (Rasulov et al. 2018; Sharkey 1990; Yang et al. 2016). Thus, under physiological conditions, dynamic leaf gas exchange observations of both A_{net} and net O₂ production (NOP) as a function of environmental conditions remain rare across diverse plant functional types and ecosystems, representing a major knowledge gap in terrestrial ecosystem carbon and oxygen cycling. Early studies demonstrated the potential of mass spectrometry to quantify leaf gross production of ¹⁶O₂ in the light simultaneously with gross ¹⁸O₂ uptake under a recirculated leaf headspace atmosphere of 21% ¹⁸O₂ (Canvin et al. 1980). This technique was used with potted tomato (*Solanum lycopersicum*) plants to demonstrate that during leaf water stress, gross oxygen production (GOP) and consumption declined together with gross CO₂ assimilation and production, suggesting that Photosystem II, the Calvin cycle and mitochondrial respiration were down-regulated (Haupt-Herting 2002). Membrane inlet mass spectrometry (MIMS) and ¹⁸O₂ isotope analysis allow differentiation between O₂ produced by Photosystem II (PSII) and that consumed by various processes, including photorespiration, mitochondrial respiration and the Mehler reaction during the water–water cycle (Allahverdiyeva et al. 2015). More recently, a new method based on measuring $\delta^{18}\text{O}$ of O₂ in air of a detached leaf equilibrated with H₂¹⁸O was used to estimate GOP and NOP determined separately from the increase in the O₂/N₂ ratio (Gauthier et al. 2018).

While few observations have been reported, the interface of environmentally controlled open-path leaf chambers to high-precision real-time oxygen sensors has opened the door to concurrent measurement of A_{net} and NOP, and thus the net assimilatory CO₂/O₂ quotient (AQ = $A_{\text{net}}/\text{NOP}$) (Cousins and Bloom 2003; LI-COR 2023). Custom differential O₂ gas analysers have been developed with two zirconium oxide cells with a precision of ± 2 ppm O₂ against a 21% O₂ background (Bloom et al. 2002) and using two O₂ fuel cells reaching a precision of ± 1 ppm O₂ (Cen, Turpin, and Layzell 2001). AQ is expected to be near 1.0 when the Calvin cycle is the dominant sink of photosynthetic energy and reducing equivalents (and when carbohydrates are used as the respiratory substrate). However, AQ values can deviate from 1.0 as a result of alternate sinks not directly coupled to CO₂ metabolism including nitrate photo-assimilation (Cousins and Bloom 2004; Smart and Bloom 2001) and potentially lipid and lignin biosynthesis (Cen, Turpin, and Layzell 2001; Cousins and Bloom 2003; Searles and Bloom 2003). Increased activity of alternative NADPH sinks like nitrate reduction can result in reductions in AQ due to a

fraction of photosynthetically produced O₂ (and electron transport rate [ETR]) not directly associated with CO₂ fixation (Bloom 2015). This effect is particularly pronounced under photorespiratory conditions when low intercellular CO₂ mole fraction (C_i) constrains RuBisCO carboxylation rates, and therefore the demand of the Calvin–Benson cycle for ATP/NADPH. Nitrate assimilation has little effect on A_{net} but enhances NOP leading to a reduction in AQ (Bloom 2015; Noctor and Foyer 1998).

While little research has studied the impact of plastidic lipid synthesis during photosynthesis on AQ (Tcherkez and Limami 2019), chloroplastic fatty acid (Tovar-Méndez, Miernyk, and Randall, 2003) and isoprenoid (Eisenreich et al. 2004) biosynthesis strictly occur in the light, requiring the photosynthetic products NADPH, ATP and glycerate-3-phosphate, which are produced by RuBisCO-catalysed carboxylation of ribulose-1,5-biophosphate (Rodrigues et al. 2020). Thus, like nitrate assimilation, photosynthetically linked lipid synthesis represents a potentially significant alternative sink of ATP/NADPH during O₂ production in chloroplasts, especially during photorespiratory conditions like high temperature which greatly enhances rates of isoprene synthesis (Jardine et al. 2014; Loreto & Sharkey 1990; Smart & Bloom 2001) due to temperature-dependent changes in substrate pool size and isoprene synthase activity (Rasulov et al. 2010). Isoprene is a particularly sensitive measure of chloroplastic ATP status, as the isoprene synthase pathway has a high effective K_m for ATP (Rasulov et al. 2014; Rasulov, Talts, and Niinemets, 2016).

Chloroplast membranes contain high amounts of the galactolipid digalactosyldiacylglycerol (DGDG) containing the fatty acid α -linolenic acid identified in early studies as a major fatty acid synthesized within chloroplasts (Bolton and Harwood 1978). During heat stress, enhanced DGDG synthesis and its incorporation into thylakoid membranes plays an important role in the ‘acquired thermotolerance’ of plants (Chen et al. 2006). However, while lipid synthesis and metabolism are widely recognized as a central component of leaf thermotolerance (Wahid et al. 2007), few studies have quantified the temperature sensitivity of lipid synthesis in chloroplasts (Tcherkez and Limami 2019), with most studies focusing on the composition of lipids present rather than their synthesis rates (Shiva et al. 2020). Isoprene is a volatile light-dependent photosynthetic lipid produced and emitted by leaves of many tree species globally as a function of temperature (Monson et al. 1992). Early pioneering studies combined gas-exchange methods with remote sensing methods and quantified leaf isoprene emissions together with CO₂/H₂O gas exchange fluxes and chlorophyll fluorescence (Loreto and Sharkey 1990). Isoprene emissions from photosynthesizing leaves of red oak (*Quercus rubra* L.) increased with light intensity, were suppressed under CO₂-free and elevated CO₂ atmospheres and were strongly enhanced with temperature (Loreto and Sharkey 1990). While isoprene synthesis depends on carbon skeletons from the Calvin cycle, isoprene production rates are primarily controlled by utilization of products from the light reactions, such as ATP and NADPH (Loreto and Sharkey 1990). This is consistent with current photosynthesis-based models of isoprene emissions, which predict that variations in isoprene emissions are primarily driven by changes in the energy status

of chloroplasts (Rasulov et al. 2009), as well as by the overall isoprenoid synthesis pathway activity (Niinemets, Rasulov, and Talts, 2021; Rasulov et al. 2014).

While the majority of carbon in leaf isoprene (C_5H_8) emissions derive from atmospheric CO_2 within minutes of photosynthesis in the light (Karl et al. 2002), alternate ‘apparent’ stored carbon sources for isoprene increase during stress (Funk, Mak, and Lerdau 2004), such as high temperature (Jardine et al. 2014). Externally supplied pyruvate and glucose have been demonstrated as effective isoprene carbon sources (Jardine et al. 2010; Kreuzwieser et al. 2002). Studies that labelled leaf isoprene with $^{13}CO_2$ suggested that pyruvate for isoprene synthesis may primarily derive from recent photosynthesis, but also partially from the import of cytosolic pyruvate generated during glycolysis (Karl et al. 2002). Studies using CO_2 -free air suggested that re-assimilation of CO_2 under photorespiratory conditions may play important roles as an ‘alternative’ carbon source for isoprene and become important as a thermotolerance mechanism during stress like high temperature and drought (Garcia et al. 2019). Although internal CO_2 and O_2 recycling in leaves are accounted for in equations describing net photosynthesis and $^{12}C/^{13}C$ fractionation, they are difficult to study (Tcherkez et al. 2017) but are known to accelerate under stress when stomata close (Ma et al. 2001). Thus, isoprene emissions may provide insight into the role of internal CO_2 and O_2 recycling in leaves under photorespiratory stress conditions such as high temperature (Voss, Sunil, Scheibe, and Raghavendra, 2013), with emission rates serving as a potential indicator of de novo lipid biosynthesis activity in chloroplasts (Jardine et al. 2020). Thus, we hypothesize that high rates of leaf isoprene emissions correspond to high carbon fluxes through the isoprenoid and fatty acid pathways, which are primarily driven by changes in NADPH and ATP availability from the light reactions.

Here, we coupled a high-precision O_2 cavity ring-down spectrometer (CRDS) and a proton transfer reaction-mass spectrometer (PTR-MS) to the sampling port of a commercial leaf gas exchange system with full environmental control and integrated fluorimeter (LI-6800 with 6 cm^2 leaf chamber). This coupling added O_2 and isoprene fluxes to CO_2/H_2O gas exchange (with chlorophyll fluorescence) for simultaneous, real-time quantification of photosynthetic traits such as ETR, A_{net} , NOP, stomatal conductance (g_s) and isoprene emissions. Furthermore, it allows the calculation of the AQ ($AQ = A_{net}/NOP$) to obtain additional information on the photosynthetic redox budget in leaves. We measured light, CO_2 and temperature responses of leaf gas exchange (CO_2 , H_2O , O_2 and isoprene) using mature leaves of California poplar (*Populus trichocarpa* Torr. & Gray) as the model tree system. The optimal temperature of GOP was measured using a method derived from Gauthier et al. (2018) via ^{18}O -water labelling.

We hypothesize that gross fluxes of photosynthesis, (photo)respiration and lipid synthesis have distinctly different temperature sensitivities and optimum temperatures. This would imply that as leaf temperature increases beyond the optimum for A_{net} and NOP, an increasing proportion of ATP and NADPH from ‘light’ reactions are used for photorespiration (Long 1991; Walker et al. 2016) and lipid synthesis (Rodrigues et al. 2020) instead of CO_2 assimilation. Due to partial stomatal

closure leading to reduced C_i , the suppression of atmospheric CO_2 uptake at high leaf temperature is partially compensated for by increased refixation of (photo)respiratory CO_2 (Voss et al. 2013) and thus enhanced CO_2/O_2 recycling (Garcia et al. 2019). We hypothesize that high temperatures will stimulate chloroplastic light-dependent lipid synthesis driven by excess NADPH and ATP not being used by the Calvin cycle (Morfopoulos et al. 2014), leading to a detectable decrease in AQ. To test this hypothesis, we quantified the temperature dependence of ETR, A_{net} , NOP, AQ and isoprene emissions as well as looked at the temperature dependence of GOP, which we hypothesized would follow the pattern of photosynthetic ETR determined from chlorophyll fluorescence.

2 | Material and Methods

2.1 | Plant Material

We used 15 potted California poplar (*Populus trichocarpa*) saplings (average height of 2 m in 15-gallon pots) obtained from Plants of the Wild (Washington State, USA) and maintained for 3 years in the South Greenhouse at the Oxford Tract Experimental Facility in Berkeley, CA, USA. The plants were regularly watered using an automated watering system and subject to standard pest control practices. The pots were filled with Supersoil planting media (Scotts Co., Marysville, OH, USA) and nitrogen was also added in the form of both nitrate (NO_3^-) and ammonium (NH_4^+) supplied using three fertilizers. Slow-release Osmocote plus was added directly to the soil during potting (240 g per pot), whereas Yara Liva $Ca(NO_3)_2$ at 90 ppm and Peters Professional at 74 ppm were mixed together in the irrigation water and applied five times per week to soil saturation. Ambient natural light was supplemented with LED lighting for the 16-h photoperiod (6:00 AM to 10:00 PM) using an Argus Titan environmental control system (Argus Controls, British Columbia, Canada). The LED lamps (10% blue and 90% red) increased light intensities at branch height by 400–1000 $\mu mol\ m^{-2}\ s^{-1}$ depending on the height and position of the top branches, with a controller automatically switching off the supplemental LED lights when the exterior light intensity was above 850 $\mu mol\ m^{-2}\ s^{-1}$.

2.2 | Leaf Gas-Exchange Measurements

Poplar branches were detached from one of the 15 trees in the greenhouse in the morning (9:00–12:00 AM), with stems immediately immersed and recut under water, and then transferred to the nearby laboratory. Harvesting branches for gas exchange studies (only one branch was removed per month per individual) did not have a negative impact on tree growth, as new leaves/branches were continuously generated by the potted trees in the greenhouse. The selected leaf to be studied for gas exchange was placed in the leaf chamber, ensuring complete coverage of the 6 or 36 cm^2 chamber window, depending on the leaf chamber used. To hydrate the branch and minimize water loss through transpiration, the branch outside the leaf chamber was immediately covered with a Mylar sheet with wet paper towels placed around the base. Therefore, only

the leaf in the chamber was actively transpiring. This was found to be important at high leaf temperatures (e.g., 40°C) to avoid leaf desiccation in the chamber associated with elevated transpiration rates. After an acclimation period (15 min), light, CO₂ or temperature response curves were measured (Figure 1). In a separate set of experiments with only the large leaf chamber, following the installation of a leaf in the chamber in darkness, the petiole was cut and placed in a solution of H₂¹⁸O for an equilibration period before measurements of a leaf temperature response (Figure 1).

For all experiments, CO₂ and H₂O gas exchange were measured under controlled environmental conditions using a portable photosynthesis system (LI-6800, LI-COR Biosciences, USA) coupled to a high-precision O₂ CRDS (Picarro Inc., USA) for O₂ and quadrupole PTR-MS (Ionicon, Austria) for isoprene measurements (Figure 1). A fraction of air exiting the leaf chamber was diverted from the LI-6800 subsampling gas port to the O₂ CRDS (90 mL min⁻¹) and PTR-MS (75 mL min⁻¹) using a 3.175-mm OD Teflon PTFE tube maintained at 50°C–60°C with a self-regulating heating tape (SLR10, Omega Engineering, USA) to prevent condensation and gas-tubing wall interactions before gas analysis by the CRDS and PTR-MS sensors. The measurement gas source for the LI-6800 was supplied externally by overblowing a T-fitting with high-purity zero air (ultra-zero air, CAS: 132259-10-0, Linde Gas) such that at least 200 mL min⁻¹ vented externally, while the remaining flow passed through a platinum catalytic converter held at 280°C (ZA30 catalyst, Aadco Instruments, USA) to oxidize any trace volatile organic compounds (VOCs) before entering the air inlet of the LI-6800.

Therefore, air delivered to the LI-6800 air inlet port was CO₂-, H₂O- and VOC-free while maintaining a constant concentration of O₂, which slightly varied from cylinder to cylinder between 20.09% and 21.03%. Leaf chamber humidity was regulated through automated balancing of air flow through the desiccant (Drierite with 10–20 mesh size CAS:778-18-9, Drierite) and humidifier (1/8 in. OD Nafion tubing immersed in ACS/HPLC water, CAS: 7732-18-5, Honeywell) to maintain the absolute humidity of the reference air at the desired setpoint of 0–12 mmol mol⁻¹. The CO₂ mole fraction inside the chamber was controlled by passing all air flow through the CO₂ scrubber (soda lime, 4–8 mesh size, CAS: 8006-28-8, Thermo Scientific), while CO₂ was supplied by an external cylinder (CAS 124-38-9, 99.9% CO₂, Praxair). When the LED lights inside the leaf chamber were switched on (1000 μmol m⁻² s⁻¹), the spectrum was set to 960 μmol m⁻² s⁻¹ red and 40 μmol m⁻² s⁻¹ blue, as recommended by the manufacturer for the fluorimeter to have just enough blue for stomatal control and to set the actinic and the fluorescence measuring beam as spectrally close as possible.

Leaf isoprene emission was measured for all gas exchange measurements using a real-time high-sensitivity quadrupole PTR-MS (with a QMZ 422 quadrupole, Balzers, Switzerland) as previously described (Jardine et al. 2014). The PTR-MS was operated with a drift tube voltage of 440 V and pressure of 1.8 mbar. For each measurement cycle lasting 24 s, the following mass-to-charge (*m/z*) ratios were monitored: *m/z* 21 (H₃¹⁸O⁺), *m/z* 37 (H₃O⁺-H₂O) and *m/z* 69 (protonated isoprene: H⁺-C₅H₈). To obtain the system background for the PTR-MS signal at *m/z* 69, measurements were made with no leaf in the

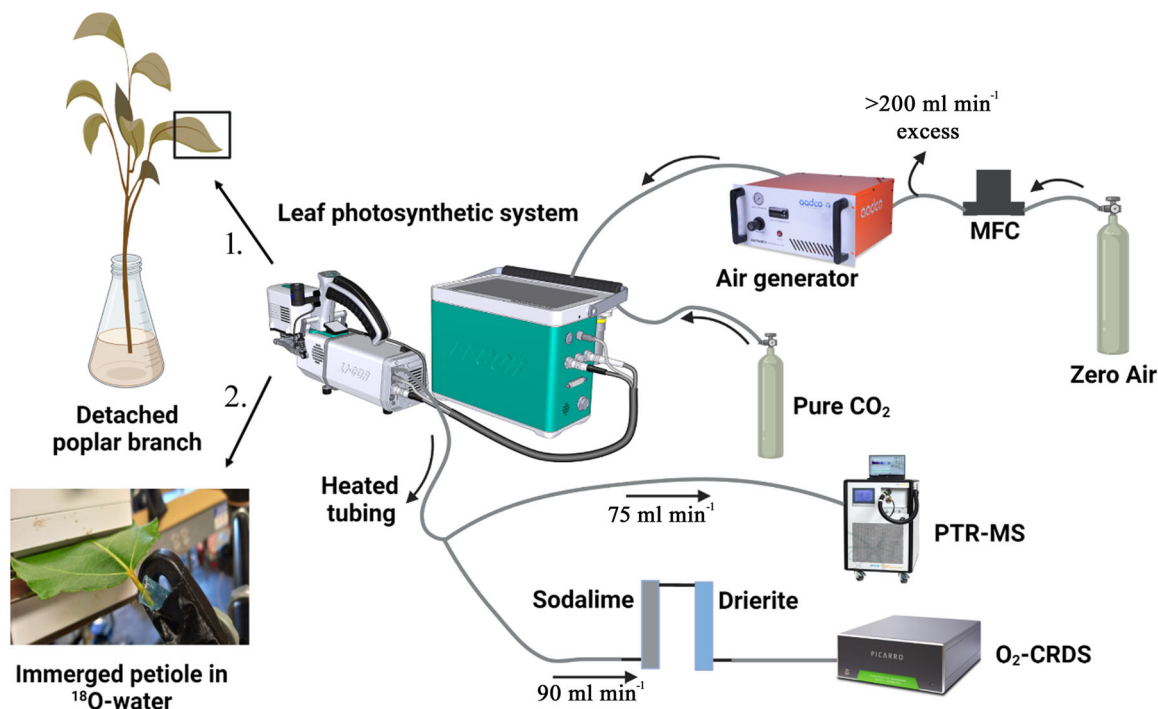


FIGURE 1 | Schematic diagram of the experimental setup for (1) real-time leaf-to-atmosphere fluxes of CO₂, H₂O, O₂ and isoprene along with chlorophyll fluorescence across environmental leaf response curves of PAR, C_i and leaf temperature, using both small and large leaf chambers, and (2) real-time leaf to atmosphere fluxes of CO₂, H₂O, and isoprene together with δ¹⁸O of leaf chamber O₂ during leaf temperature response curves, using the large leaf chamber. Note that chlorophyll fluorescence was only quantified using the small leaf chamber. Note, the air flow rate through the small leaf chamber (6 cm²) varied between 323 and 363 mL min⁻¹ (depending on the leaf), while the large chamber (36 cm²) maintained the same air flow rate (538 mL min⁻¹) for all leaves studied (see Section 4).

chamber both before and after every environmental response curve with a leaf. Once a leaf was installed in the chamber, isoprene concentrations inside the leaf chamber were calculated by subtracting the background m/z 69 and applying the calibration sensitivity of the m/z 69 signal to isoprene determined separately through dynamic dilution of 1.0 ppm isoprene standard. A similar procedure was used to determine the background concentration of O_2 (see section below on NOP calculation).

In these experiments, two different leaf chambers were used with distinct advantages and disadvantages (Supporting Information S1: Figure S1). The smaller leaf chamber (6 cm²) had the added advantage of including an integrated chlorophyll fluorimeter (6800-01A, LI-COR Biosciences) together with H₂O and CO₂ gas exchange. Due to the rerouting of a fraction of the outlet air for simultaneous measurements of O₂ and isoprene concentrations, and small leaks that formed between the gasket and the leaf/petiole, over-pressurizing the leaf chamber (0.1 kPa) with an optimized flow rate of 323–363 mL min⁻¹ (240–270 μmol mol⁻¹) ensured high O₂ gradients while maintaining sufficient flow for O₂ (90 mL min⁻¹), isoprene (75 mL min⁻¹) and CO₂ + H₂O (158–198 mL min⁻¹) measurements (Supporting Information S1: Figure S1a). Chlorophyll fluorescence data were simultaneously recorded with gas exchange data during light, CO₂ and temperature response curve measurements with an integrated multiphase flash fluorimeter system (model 6800-01A, LI-COR Biosciences). To measure the light-adapted maximum fluorescence yield, F_m' , an actinic light pulse of 1000 μmol m⁻² s⁻¹ was applied for 1 s. The fluorimeter measurement light frequency was 50 Hz in the dark and 1 kHz in light, and 250 kHz during saturating flash. For steady-state fluorescence measurements (F_s), 15 s chlorophyll fluorescence signal averaging was used (100 Hz data output rate with a margin of 5 averaged points before and after flash). Photosynthetic ETR (μmol e⁻ m⁻² s⁻¹) was calculated according to Equation (1), where f is the fraction of the quantum absorbed and used by Photosystem II, with a value of 0.5 used for C₃ plants (Earl and Tollenaar 1998), photosynthetically active radiation (PAR) is the incident photon flux density (μmol m⁻² s⁻¹), and α_{leaf} is the fraction of light absorbed by the leaf (0.87). Although α_{leaf} was not experimentally determined, both the blue and red wavelengths are known to be strongly absorbed by green leaves, with typical values between 0.84 and 0.90. For example, when leaf light absorption was quantified for four broad leaf tree species, α_{leaf} values ranged between 0.87 and 0.92 (Kang et al. 2020)

$$ETR = \frac{F_m' - F_s}{F_m'} \times f \times PAR \times \alpha_{leaf}. \quad (1)$$

A larger leaf chamber with an integrated LED light source (model 6800-03 LI-COR Biosciences) was also used with the advantage of enclosing a much larger area of enclosed leaf (36 cm²). This allowed for a higher flow rate of air to be delivered to the leaf chamber (538 mL min⁻¹ or 400 μmol s⁻¹). While lacking a fluorimeter, the large leaf chamber can control leaf temperature and the actinic light spectra, which was set identically to the small chamber (960 μmol m⁻² s⁻¹ red and 40 μmol m⁻² s⁻¹ blue) (Supporting Information S1: Figure S1b).

2.3 | Photosynthesis, ETR and Isoprene Emission Responses to Environmental Drivers

2.3.1 | Light Response Curves

Photosynthetic light response curves were measured at a constant leaf temperature (32°C), leaf chamber CO₂ mole fraction of 400 μmol mol⁻¹ and reference (inlet) air humidity of 12 mmol mol⁻¹. For both large and small chambers, after 30 min dark acclimation (PAR: 0 μmol m⁻² s⁻¹), leaf gas exchange and chlorophyll fluorescence (small chamber only) responses to light intensity were measured. This included a sequence of increasing followed by decreasing PAR (0, 200, 400, 600, 800, 1000, 1200, 1400, 1600, 1200, 800, 400, 100, 50, 40, 30, 20, 10 and 0 μmol m⁻² s⁻¹). Total time duration for the measurement of a light response curve was 200 min. Three replicate light response curves were collected using the small chamber with gas exchange and chlorophyll fluorescence and two replicate light response curves were collected using the large chamber with gas exchange only. For each replicate, a branch from a different tree (5 out of 15 total) was used.

2.3.2 | C_i Response Curves

The response of leaf gas exchange to intercellular CO₂ mole fraction (C_i) was measured by varying the reference CO₂ mole fraction entering the leaf chamber while maintaining constant leaf temperature (32°C), PAR (1000 μmol m⁻² s⁻¹) and reference air humidity (10 mmol mol⁻¹). For both small and large leaf chambers, after 30 min light acclimation (PAR: 1000 μmol m⁻² s⁻¹), leaf gas exchange and chlorophyll fluorescence (small chamber only) response curves to CO₂ were measured. This included a sequence of decreasing followed by increasing reference CO₂ mixing ratios (400, 350, 300, 250, 200, 150, 125, 100, 75, 50, 25, 0, 50, 100, 150, 200, 250, 300, 400, 500, 600, 700, 800, 900 and 1000 ppm). Total time duration for a single C_i response curve was 160 min. Four replicate C_i response curves were collected using the small chamber and three replicate C_i response curves were collected using the large chamber. For each replicate, a branch from a different tree (7 out of 15 total) was used.

2.3.3 | Leaf Temperature Response Curves

Leaf temperature response curves were measured with varying leaf temperature at a constant CO₂ mixing ratio in the leaf chamber (C_a , 400 μmol mol⁻¹) and inlet (reference) air humidity (0–8 mmol mol⁻¹). To prevent condensation in the large leaf chamber, dry inlet air (with 0 mmol mol⁻¹ water vapour) was supplied, while in the small leaf chamber, the shorter gas residence time allowed us to use inlet air with a humidity of 8 mmol mol⁻¹ (see also Section 4). For both large and small leaf chambers, after 30 min dark acclimation (PAR: 0 μmol m⁻² s⁻¹) at 25°C leaf temperature, leaf gas exchange (both chambers) and chlorophyll fluorescence (small chamber only) responses to leaf temperature were measured. The sequence started with leaf dark respiration measurements at 25.0°C (PAR: 0 μmol m⁻² s⁻¹). Following a 20-min period of light acclimation, measurements of

the temperature response curve in the light (PAR: 1000 $\mu\text{mol m}^{-2} \text{s}^{-1}$) were initiated with increasing leaf temperatures (25°C, 27.5°C, 30°C, 32.5°C, 35°C, 37.5°C and 40°C). After the temperature response curve measurements, incident light was switched off to record leaf dark respiration at 40°C. Total time duration for a leaf temperature response curve measurement was 120 min. Eight replicate leaf temperature response curves were collected using the small chamber. For each replicate, a branch from a different tree (8 out of 15 total) was utilized. In addition, seven replicate leaf temperature response curves were collected using the large chamber (7 out of 15 total).

2.4 | Leaf H_2^{18}O Labelling

To determine optimal temperature of GOP, leaf responses to temperature were monitored using the large leaf chamber with detached poplar leaves equilibrated with a solution of H_2^{18}O water (seven replicate temperature curves from individual replicate trees). The O_2 CRDS was switched into isotope mode, where $\delta^{18}\text{O}$ in O_2 of the leaf headspace air was measured with <1‰ precision using 7-min averages. Water enriched in H_2^{18}O ($\delta^{18}\text{O}$ value of +8.000‰ relative to Vienna Standard Mean Ocean Water, V-SMOW) was prepared by diluting 10 atom % H_2^{18}O water (CAS:14314-42-2, Sigma-Aldrich) with HPLC grade water. The leaf was detached from the branch and the petiole was immediately recut under H_2^{18}O -enriched water, then placed in the large chamber under constant light (PAR: 1000 $\mu\text{mol m}^{-2} \text{s}^{-1}$), leaf temperature (32°C) and leaf chamber CO_2 mole fraction (C_a , 400 $\mu\text{mol mol}^{-1}$). $\delta^{18}\text{O}$ of O_2 of air inside the leaf chamber was measured before, during and after gas exchange experiments with a leaf (before and after measured with no leaf in the chamber). Concurrently, continuous measurement of leaf isoprene emission was measured using PTR-MS (Figure 1). Equilibration of the leaf with ^{18}O -enriched water occurred for 2–3 h, during which the $\delta^{18}\text{O}$ of O_2 values reached a steady state, indicating the turnover of all non-static leaf water pools. Following the equilibration period, the leaf temperature response curve was measured using the same protocol as that of attached leaves (see above).

2.5 | Real-Time Measurement of Leaf NOP

CO_2 and H_2O were quantitatively scrubbed from the air exiting the leaf chamber by passing it through indicating soda lime (replaced monthly), followed by indicating Drierite (replaced daily) using separate chemical tube assemblies (LI-COR Inc., Part # 9960-093). For all O_2 measurements, H_2O remained below 0.1%. Following the scrubbing of CO_2 and H_2O from the diverted air flow exiting the leaf chamber, an infrared laser-based CRDS (Picarro G2207-i, $\text{O}_2/\text{H}_2\text{O}$, USA) was used for continuous high-precision measurement of O_2 mole fraction or $\delta^{18}\text{O}$ values in O_2 (Figure 1). In fact, the CRDS could be operated in one of two different modes: high-precision concentration and isotopic ratio modes. In concentration mode, the O_2 mole fraction was measured with <2 ppm precision using 7-min averages. O_2 reference mole fraction measurements were made with an empty chamber before and after all leaf environmental response curves and

used to calculate the change in O_2 concentrations due to leaf gas exchange (ΔO_2). Small drifts in measured O_2 inlet mole fraction during the response curves, as determined from measurements without a leaf in the chamber before and after the environmental response curves, were <20 ppm O_2 (see example raw data Supporting Information S1: Figure S2). This drift in reference leaf chamber O_2 concentrations is attributed to the CRDS itself and was subtracted from the headspace O_2 concentrations when a leaf was in the chamber. That way, the difference in O_2 mole fractions between the leaf chamber and reference air (ΔO_2) could be determined in real time during the environmental response curves. Leaf NOP ($\mu\text{mol m}^{-2} \text{s}^{-1}$) fluxes were calculated using Equation (2), where μ is the air flow rate entering the leaf chamber (mol air s^{-1}), ΔO_2 is the difference in oxygen mole fraction between leaf chamber and reference air corrected for CRDS drift ($\mu\text{mol mol}^{-1}$) and S is leaf surface area (0.0006 or 0.0036 m^2) inside the chamber. Note that, due to the quantitative scrubbing of CO_2 and H_2O in the air exiting the leaf chamber just before making O_2 measurements by the CRDS, corrections associated with air flow rate due to transpiration and photosynthesis were not necessary

$$\text{NOP} = \mu \frac{\Delta\text{O}_2}{S}. \quad (2)$$

To determine the average $\text{AQ} = A_{\text{net}}/\text{NOP}$ for each environmental leaf response curve, a linear regression analysis was performed with A_{net} (y -axis) plotted against NOP (x -axis). Highly linear correlations were observed in all cases, with the slope of the regression representing AQ. In addition to AQ values determined from the slope of the linear correlations from each leaf environmental response curve, mean AQ values were also determined by directly dividing the mean values of A_{net} by NOP for each value of PAR, C_i and leaf temperature.

3 | Results

3.1 | Light Response

A_{net} and NOP increased as a function of PAR together with ETR and isoprene emissions. Whereas ETR saturated around 1000 $\mu\text{mol m}^{-2} \text{s}^{-1}$ PAR, A_{net} , NOP and isoprene emissions continued to increase with light up to the highest intensity (1600 $\mu\text{mol m}^{-2} \text{s}^{-1}$ PAR). An example light response curve is shown in Figure 2 and summarized in Supporting Information S1: Figure S3 for all replicate experiments. A_{net} showed a higher magnitude relative to NOP (Figure 2b). This resulted in an $\text{AQ} = A_{\text{net}}/\text{NOP}$ higher than unity ($\text{AQ} = 1.3$; Figure 2c). In this example, dark CO_2 evolution was 3.8 $\mu\text{mol m}^{-2} \text{s}^{-1}$, while dark oxygen consumption was 2.5 $\mu\text{mol m}^{-2} \text{s}^{-1}$. Similarly, under saturating light (1600 $\mu\text{mol m}^{-2} \text{s}^{-1}$ PAR), A_{net} (18.4 $\mu\text{mol m}^{-2} \text{s}^{-1}$) was higher than NOP (15.5 $\mu\text{mol m}^{-2} \text{s}^{-1}$) (Figure 2b,c). At low light intensity (0–200 $\mu\text{mol m}^{-2} \text{s}^{-1}$) a linear response was observed with A_{net} , NOP and ETR (Figure 2b and Supporting Information S1: Figures S3). g_s and transpiration rate (E) also increased with PAR, reaching a maximum value (g_s : 0.35 $\text{mol m}^{-2} \text{s}^{-1}$; E : 8.0 $\text{mmol m}^{-2} \text{s}^{-1}$) at 1200 $\mu\text{mol m}^{-2} \text{s}^{-1}$. At high light, both g_s and E decreased

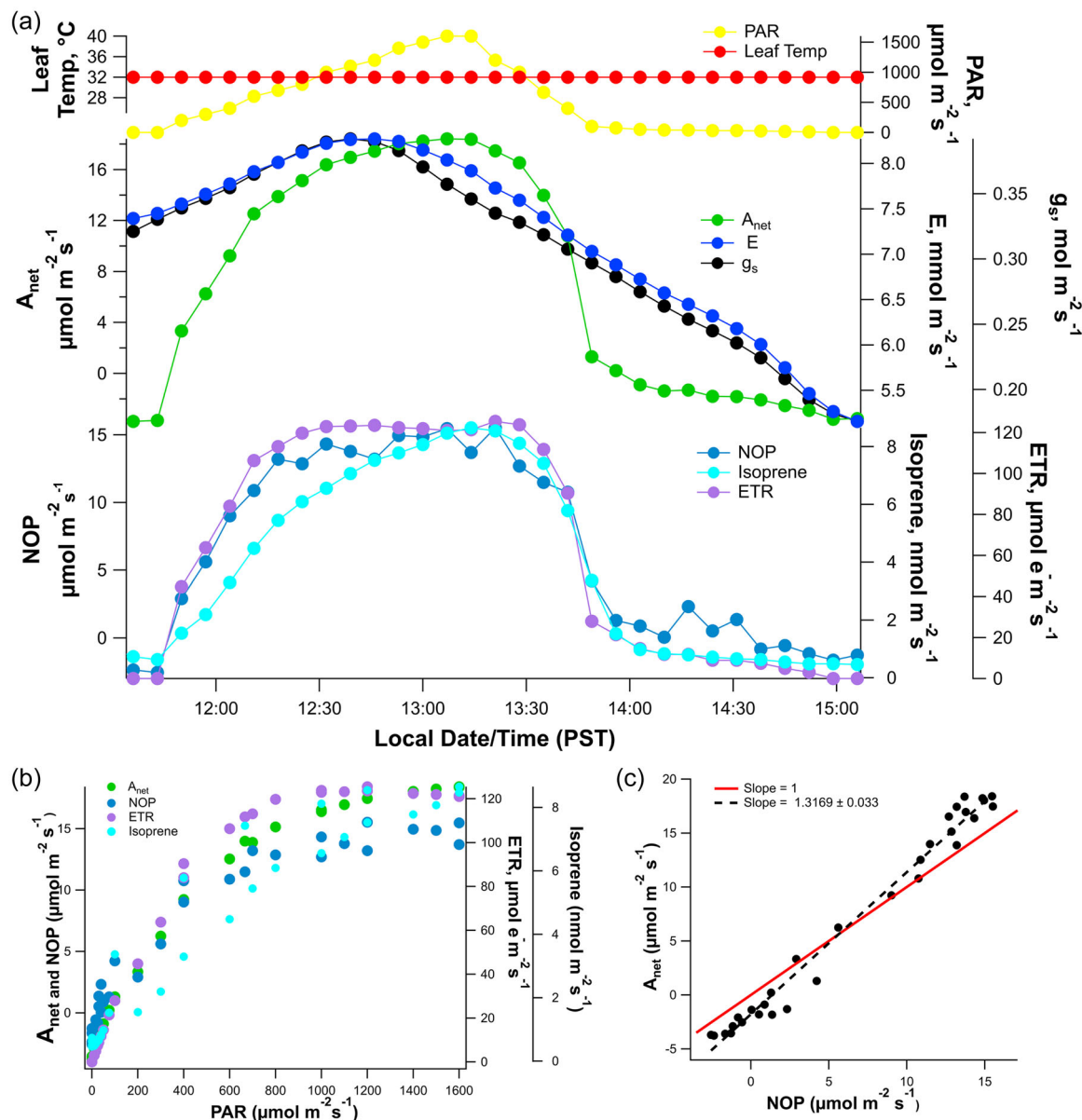


FIGURE 2 | (a) Example real-time leaf-gas exchange fluxes of A_{net} , NOP and isoprene emissions, together with chlorophyll fluorescence-derived ETR during controlled light response curves (photosynthetically active radiation, PAR), under constant leaf temperature (32°C) and leaf chamber headspace CO₂ concentrations (400 ppm) collected using the 6 cm² leaf chamber with integrated chlorophyll fluorimeter. (b) A_{net} and NOP and ETR and isoprene emissions plotted as a function of PAR. (c) Linear regression between A_{net} and NOP. Note the slope of the regression as well as the 1:1 line.

TABLE 1 | Assimilatory quotient (AQ = $A_{\text{net}}/\text{NOP}$) determined as the slope from linear regressions between net CO₂ exchange (A_{net}) and net oxygen production (NOP) during leaf gas exchange response curves to light, leaf internal CO₂ concentrations (C_i) and leaf temperature (under constant light) for both large and small dynamic leaf chambers.

Leaf chamber	AQ (light)	AQ (C_i)	AQ (temperature)
Large chamber	1.223 ± 0.003 ($n = 2$)	1.272 ± 0.016 ($n = 3$)	0.975 ± 0.330 ($n = 7$)
Small chamber	1.268 ± 0.057 ($n = 3$)	1.192 ± 0.082 ($n = 4$)	0.793 ± 0.226 ($n = 8$)
Large + small chamber	1.250 ± 0.047 ($n = 5$)	1.227 ± 0.073 ($n = 7$)	0.865 ± 0.275 ($n = 15$)

Note: AQ values are shown as mean ± 1 standard deviation, with n indicating the number of replicate leaf response curves.

slightly. AQ values determined using the small leaf chamber (6 cm², AQ = 1.26 ± 0.06) were similar to those determined with the large leaf chamber (36 cm², AQ = 1.22 ± 0.01) (Table 1).

3.2 | CO₂ Response

Response curves to intercellular CO₂ mole fraction (C_i) are shown in Figure 3 and summarized in Supporting Information

S1: Figure S4 for all of the replicate experiments. Both A_{net} and NOP increased with C_i , although A_{net} showed a larger magnitude at both low (more negative) and high C_i (more positive) than NOP. Across all C_i response curves, AQ values determined using the small leaf chamber (6 cm^2 , $\text{AQ} = 1.23 \pm 0.08$) were similar to those determined using the large leaf chamber (36 cm^2 , $\text{AQ} = 1.27 \pm 0.02$) (Table 1). For the example shown in Figure 3, as reference CO_2 entering the leaf chamber declined from 400 to $0 \mu\text{mol mol}^{-1}$, C_i declined from 320 to $31 \mu\text{mol mol}^{-1}$. A_{net} , NOP and ETR strongly declined by 122%, 122% and 59%, respectively, with A_{net} and NOP becoming negative below a C_i of $56 \mu\text{mol mol}^{-1}$ (the CO_2 compensation point for A_{net} and NOP), such that the leaf became a net source of CO_2 and sink of

O_2 in the light. At the lowest C_i ($31 \mu\text{mol mol}^{-1}$), net CO_2 evolution ($3.8 \mu\text{mol m}^{-2} \text{ s}^{-1}$) was slightly higher than net oxygen consumption ($2.2 \mu\text{mol m}^{-2} \text{ s}^{-1}$). In contrast, isoprene emissions were stimulated as C_i declined from 320 to $56 \mu\text{mol mol}^{-1}$ (67% increase), followed by a decline as C_i reached the lowest value, $31 \mu\text{mol mol}^{-1}$ (19% decrease). As reference CO_2 entering the leaf chamber increased above 400 ppm, A_{net} , NOP, and ETR strongly increased reaching a photosynthetic plateau for C_i above $588 \mu\text{mol mol}^{-1}$. In contrast, isoprene emissions were suppressed at elevated C_i , decreasing by 87% from 207 to $868 \mu\text{mol mol}^{-1}$. Taken as a whole, A_{net} , NOP and ETR were much more sensitive to changes in C_i than isoprene emissions.

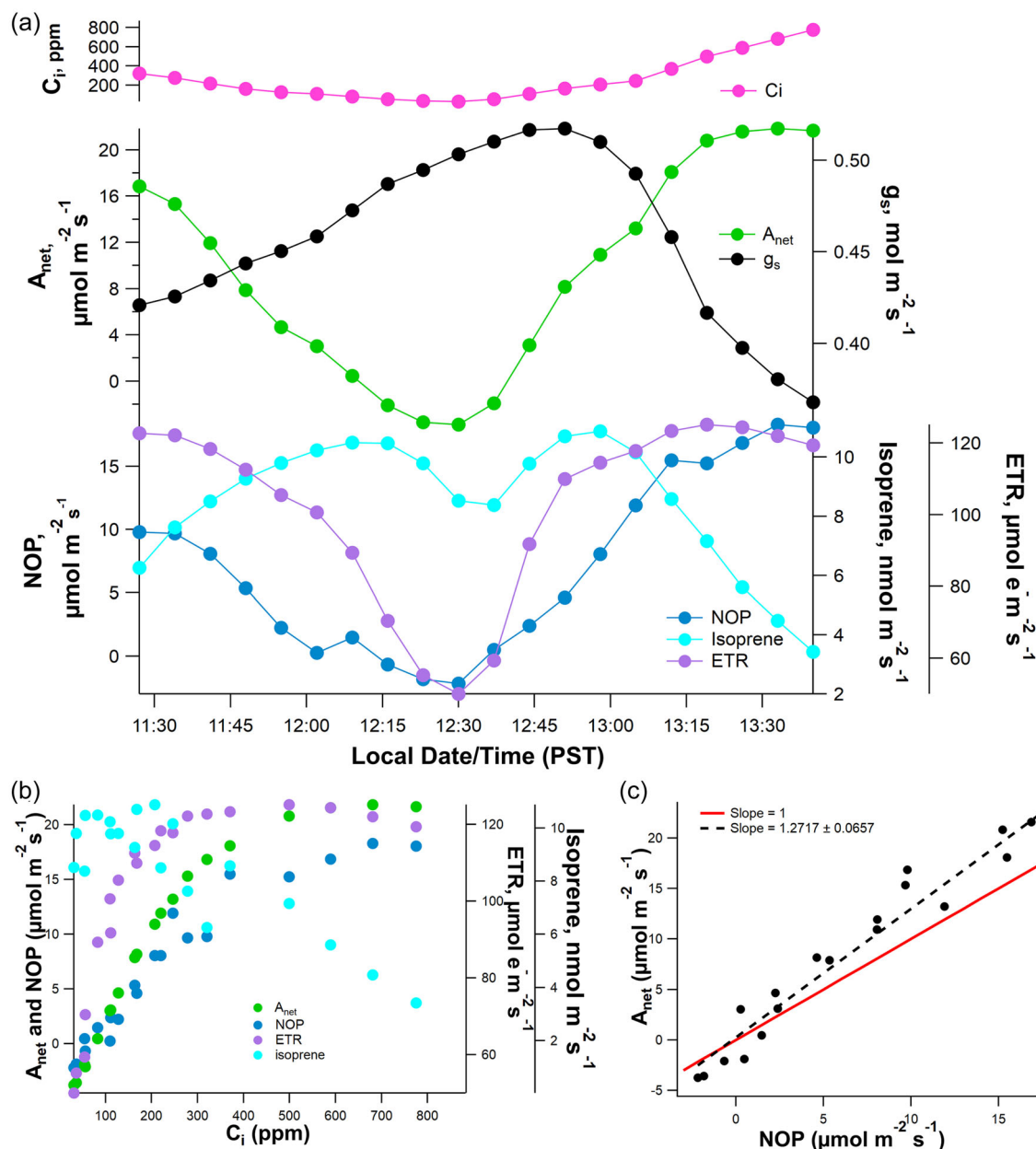


FIGURE 3 | (a) Example real-time leaf-gas exchange fluxes of A_{net} , NOP and isoprene emissions together with ETR during controlled C_i response curves under constant leaf temperature (32°C) and PAR ($1000 \mu\text{mol m}^{-2} \text{ s}^{-1}$) collected using the 6 cm^2 leaf chamber with integrated chlorophyll fluorimeter. (b) A_{net} and NOP together with ETR and isoprene emissions plotted as a function of C_i . (c) Linear regression between A_{net} and NOP. Note the slope of the regression as well as the 1:1 line.

3.3 | Temperature Response

An example leaf temperature response curve is shown in Figure 4, with a summary of replicates presented in Supporting Information S1: Figure S5. In the light at 25°C, A_{net} , NOP and ETR showed high values, while isoprene emissions remained low but detectable ($< 0.5 \text{ nmol m}^{-2} \text{ s}^{-1}$). As leaf temperature increased in the light, A_{net} and NOP reached maximum values near 31°C and then decreased slightly at higher temperatures. In contrast, ETR continued to increase in the light to a

maximum near 36°C, while isoprene emissions continued to increase up to the highest leaf temperature used (40°C). Upon switching off the light at the highest leaf temperature (40°C), A_{net} and NOP rapidly declined and became negative while isoprene emission was nearly suppressed. In all leaves studied, an increase in leaf dark respiration (A_{net} and NOP) was observed at 40°C relative to 25°C. In contrast to what was observed with light and C_i response curves, leaf temperature response curves in the light showed AQ values less than unity, with relatively higher variability ($AQ = 0.865 \pm 0.275$; Table 1).

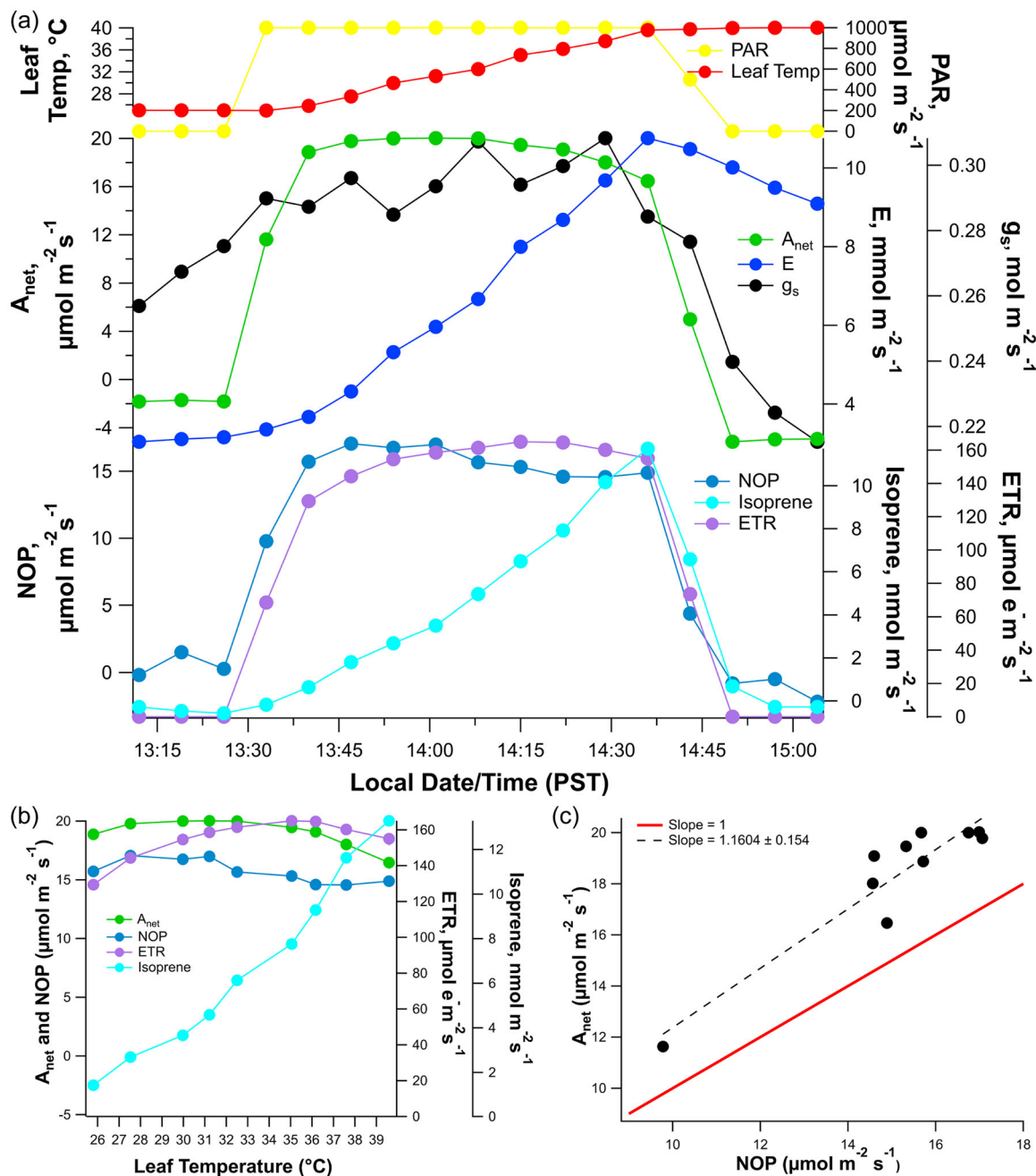


FIGURE 4 | (a) Example real-time leaf-gas exchange fluxes of A_{net} , NOP and isoprene emissions together with ETR during controlled leaf temperature response curves under constant leaf headspace enclosure CO_2 (400 ppm) and PAR ($1000 \mu\text{mol m}^{-2} \text{ s}^{-1}$) collected using the 6 cm^2 leaf chamber with integrated chlorophyll fluorimeter. (b) A_{net} and NOP together with ETR and isoprene emissions plotted as a function of leaf temperature. (c) Linear regression between A_{net} and NOP in the light. Note the slope of the regression as well as the 1:1 line shown.

3.4 | Temperature Response Curves with ^{18}O -water

The temperature dependence of GOP was assessed using detached mature poplar leaves placed in the large (36 cm^2) chamber in the light, with the petiole immersed in ^{18}O -enriched water (Figure 5 and summarized in Supporting Information S1: Figure S6). In the example shown in Figure 5, during the equilibration period (incubation in ^{18}O -enriched water) in the light ($1000\ \mu\text{mol m}^{-2}\text{ s}^{-1}$) at 30°C , the $\delta^{18}\text{O}$ of outlet O_2 increased from the background value (ca. $+11\text{‰}$) and reached $+21\text{‰}$ within 2 h in the steady state. During this equilibration period, leaf isoprene emissions also increased but reached a steady state much faster (within 15 min). Upon switching off the light and reducing the leaf temperature to 25°C , $\delta^{18}\text{O}$ of outlet O_2 values quickly returned to background values of $+12\text{‰}$. When the light was switched on again at 25°C ,

$\delta^{18}\text{O}$ values reached $+20\text{‰}$ and increased with leaf temperature up to a maximum of $+23\text{‰}$ at 37.5°C , and then decreased slightly at the highest leaf temperature (40°C). When the light was switched off at 40°C (end of the temperature response curve), $\delta^{18}\text{O}$ of outlet O_2 rapidly returned to the background value of $+12\text{‰}$. Although A_{net} showed a similar optimum leaf temperature of (30°C) to that of non-detached leaves (Figure 4b vs. Figure 5b), the optimum temperature of $\delta^{18}\text{O}$ was much higher (37.5°C).

3.5 | Optimal Temperature of Photosynthetic Parameters

Data on optimal temperature (T_{opt}) of A_{net} , NOP, GOP, ETR and isoprene emissions were compiled from the temperature response curves using the small ($n = 8$) and large ($n = 7$) leaf

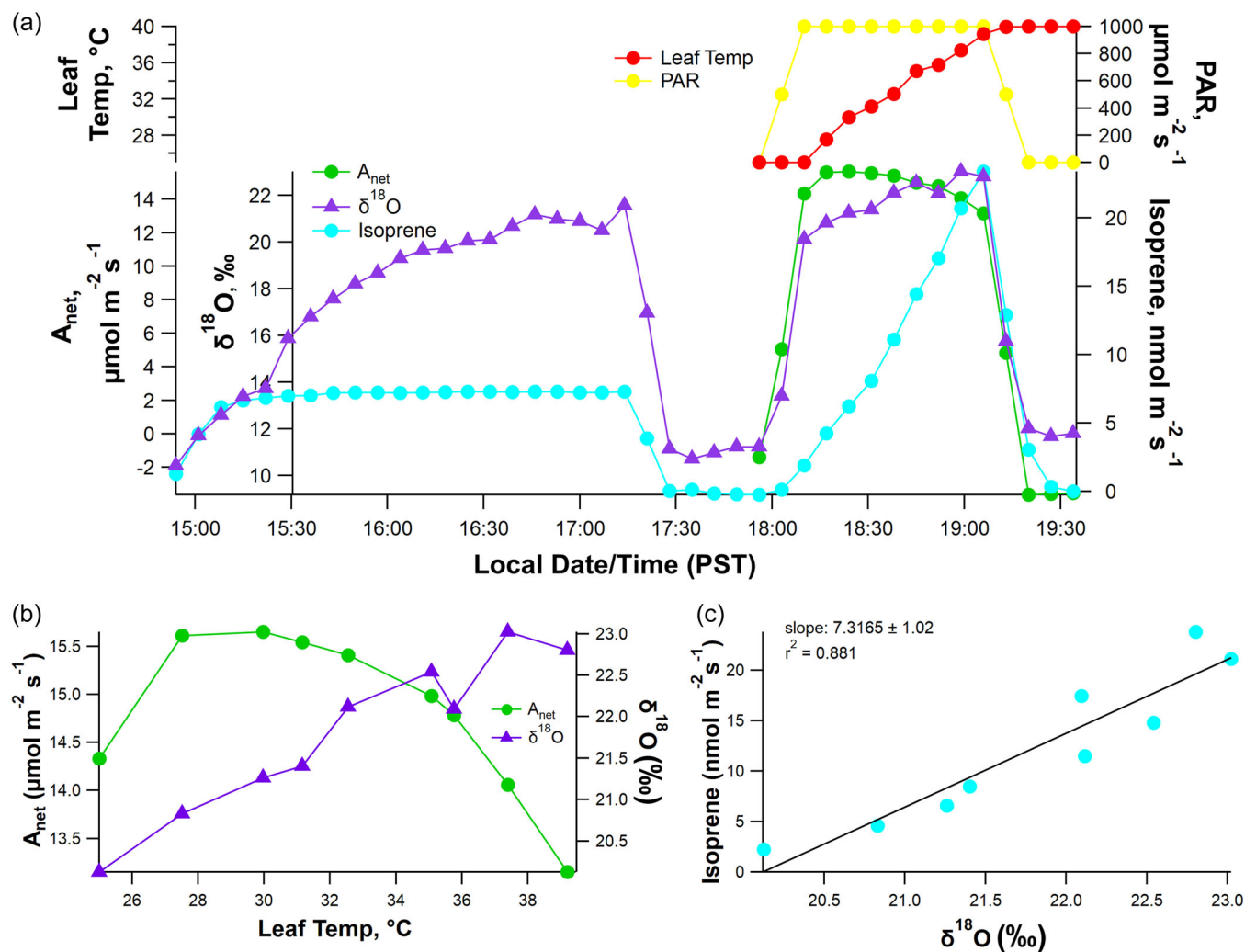


FIGURE 5 | Example dynamics of ^{18}O -labelled O_2 evolution in the light as a function of leaf temperature from a detached poplar leaf equilibrated with ^{18}O -water ($\delta^{18}\text{O}$ 8000‰) using the 36 cm^2 leaf chamber. Pretreatment occurred under constant PAR ($1000\ \mu\text{mol m}^{-2}\text{ s}^{-1}$), leaf temperature (32°C) and leaf enclosure headspace CO_2 (400 ppm). (a) Example real-time leaf-gas exchange fluxes of A_{net} and isoprene emissions together $\delta^{18}\text{O}$ in headspace O_2 during a controlled leaf temperature response curves under constant leaf headspace enclosure CO_2 (400 ppm). Following equilibration, the light was switched off (PAR $0\ \mu\text{mol m}^{-2}\text{ s}^{-1}$) and the leaf temperature was reduced to 25°C . Following measurements of dark gas parameters, PAR was returned to $1000\ \mu\text{mol m}^{-2}\text{ s}^{-1}$ and the leaf temperature response curve was initiated (25°C – 40°C). Finally, the light was switched off to determine the dark gas exchange rates at 40°C leaf temperature, (b) A_{net} and $\delta^{18}\text{O}$ of O_2 plotted as a function of leaf temperature and (c) linear regression between isoprene emissions and $\delta^{18}\text{O}$ of O_2 across leaf temperature in the light (PAR, $1000\ \mu\text{mol m}^{-2}\text{ s}^{-1}$). Note the slope of the regression as well as the 1:1 line shown.

chambers as well as the large leaf chamber during ^{18}O -water labelling ($n = 7$). As summarized in Table 2 and graphically in Figure 6, A_{net} and NOP showed mean \pm SD optimal temperatures of $31.0 \pm 3.1^\circ\text{C}$ and $31.0 \pm 3.4^\circ\text{C}$, respectively. ETR and GOP showed distinctively higher temperature optima of $35.0 \pm 1.8^\circ\text{C}$ and $34.9 \pm 1.8^\circ\text{C}$, respectively. Isoprene emission had the highest temperature optimum at $38.9 \pm 1.0^\circ\text{C}$. Despite a suppression in g_s at high temperatures (g_s temperature optima of $33.0 \pm 5.7^\circ\text{C}$), transpiration continued to increase with leaf temperatures (T_{opt} of 38.9 ± 2.6).

4 | Discussion

Using California poplar (*Populus trichocarpa*) as a model tree species, we added NOP and isoprene fluxes as well as $\delta^{18}\text{O}$ in O_2 to $\text{CO}_2/\text{H}_2\text{O}$ gas exchange with chlorophyll fluorescence and measured light, CO_2 and temperature response curves. For a detailed discussion of the specific leaf chambers, flow rates and O_2 concentration gradients, see Supporting Information S1: Discussion, 'Pros and cons of coupling gas exchange to O_2 and isoprene flux measurements'. It should be noted that we focused here on short-term leaf responses to changes in environmental variables (including temperature) using controlled leaf chambers, and thus our study does not include potential longer term acclimation effects to growth temperature (Hikosaka et al. 2006), light (Laisk et al. 2002) and CO_2 (Wolfe et al. 1998). For example, while we determined that the optimal temperature that maximizes both A_{net} and NOP (T_{opt}) is 31°C (Table 2), previous studies have found that T_{opt} may increase with increasing growth temperature (Hikosaka et al. 2006). *Populus trichocarpa* has a very broad and extensive natural distribution in western North America in the foothills of the Sierra Nevada range, Northern California and throughout much of Oregon and Washington, including both sides of the Cascade range, extending into western Canada and north to Alaska as well as east to Alberta, Montana, Utah and Wyoming (USDA 2024). Maximum daytime air temperature in Poplar forests in the western United States and Oregon has been reported to vary between 15.5°C and 47.2°C (Niemiec 1995). Although leaf temperature is not always measured, leaves can be 1°C – 7°C warmer than air temperature during the day (Gimenez et al. 2019; Monson et al. 2020). Therefore, depending on the local

climate and acclimation processes, T_{opt} may be regularly surpassed during the summer growing season at some sites, especially during summer heat waves such as the one in the US Pacific Northwest in June 2021, which broke all-time maximum temperature records by more than 5°C , and set a new record high temperature of 49.6°C in Canada (White et al. 2023). Monthly average climatological data maintained by the Western Regional Climate Center at The Poplars site in Oregon (Site 358420), USA showed a monthly average high air temperature in August of 29.5°C , but with daily maximum temperatures reaching up to 40°C (WRCC, 1941–2012). At a poplar plantation in a semi-arid site in Arizona during the summer growing season (June–September), continuous canopy temperature observations during the summer months of 2014 showed that leaf temperatures surpassed 31°C almost every day and reached up to $\sim 40^\circ\text{C}$ on many days (Monson et al. 2020).

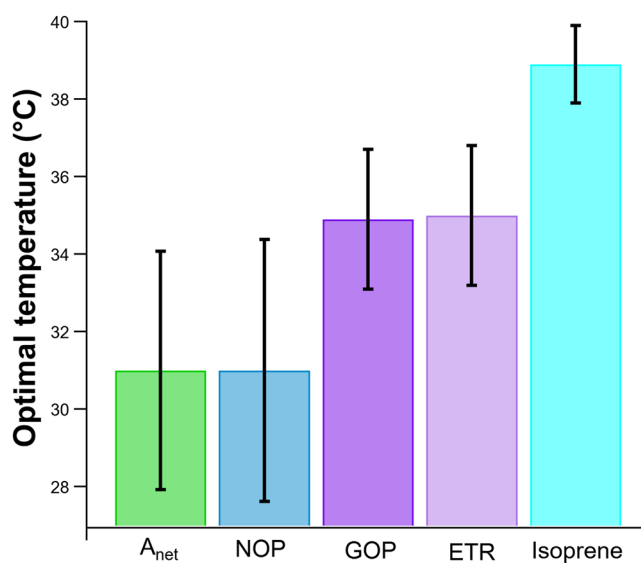


FIGURE 6 | Average optimum temperature (T_{opt}) of net CO_2 assimilation (A_{net}), net oxygen production (NOP), gross oxygen production (GOP), photosynthetic electron transport rates (ETR) and isoprene emission during controlled leaf temperature response curves ($n = 15$) using the small ($n = 8$) and large ($n = 7$) leaf chambers. Vertical error bars represent ± 1 standard deviation. T_{opt} for GOP was only determined with the large chamber (36 cm^2) and T_{opt} for ETR was only determined with the small chamber (6 cm^2).

TABLE 2 | Optimal temperature (T_{opt}) of leaf gas exchange characteristic and electron transport and isoprene emission determined from the leaf temperature response curves.

Parameter	T_{opt} ($^\circ\text{C}$)	Symbol (unit)	Instrument
Net photosynthesis	31.0 ± 3.1	A_{net} ($\mu\text{mol m}^{-2} \text{s}^{-1}$)	LI-6800
Net oxygen production	31.0 ± 3.4	NOP ($\mu\text{mol m}^{-2} \text{s}^{-1}$)	CRDS in O_2 concentration mode
Stomatal conductance	33.0 ± 5.7	g_s ($\text{mol m}^{-2} \text{s}^{-1}$)	LI-6800
Photosynthetic electron transport rate	35.0 ± 1.8	ETR ($\mu\text{mol m}^{-2} \text{s}^{-1}$)	LI-6800
Gross oxygen production	34.9 ± 1.8	$\delta^{18}\text{O}$ in O_2 (‰)	CRDS in $\delta^{18}\text{O}$ mode
Transpiration	38.9 ± 2.6	E ($\text{mmol m}^{-2} \text{s}^{-1}$)	LI-6800
Leaf isoprene emissions	38.9 ± 1.0	Isoprene ($\text{nmol m}^{-2} \text{s}^{-1}$)	PTR-MS

4.1 | Apparent AQ

Across light, CO₂ and temperature response curves, A_{net} and NOP were tightly coupled and highly positively correlated, enabling the determination of apparent AQ values ($\text{AQ} = A_{\text{net}}/\text{NOP}$) for each leaf experiment. For the light and CO₂ response curves, A_{net} displayed a ~30% higher magnitude compared with NOP during conditions of low or negative net photosynthesis rates (darkness and low C_i) and during conditions of high net photosynthesis rates (e.g., saturating light and CO₂) (Figures 2 and 3 and Supporting Information S1: Figures S3 and S4). This caused the values of AQ to be higher than 1.0. When all leaf response curves were analysed for AQ values (Table 1), with means compared using a *t*-test, no statistically significant difference was observed between AQ values determined from the light and C_i response curves (two-tailed *p* value of 0.5524). In contrast, statistically significant differences were observed between AQ values from the light and temperature response curves (two-tailed *p* value of 0.0067) and C_i and temperature response curves (two-tailed *p* value of 0.0029). This suggests that the mean leaf AQ, as determined here by regressing all A_{net} versus NOP fluxes obtained during each environmental response curve, did not depend on light or C_i (driven by changes in leaf headspace CO₂ concentrations) but appeared to be suppressed as leaf temperature increase in the light. This is consistent with AQ values determined by directly dividing the mean values of A_{net} by NOP for each value of PAR, C_i and leaf temperature, respectively. That is, while mean AQ values determined as a function of environmental variables remained relatively constant as a function of PAR (Supporting Information S1: Figure S3) or C_i (Supporting Information S1: Figure S4), they appeared to decline as a function of leaf temperature (Supporting Information S1: Figure S5).

AQ may deviate from 1.0 when significant activity of alternative electron transport processes occurs that are not involved in CO₂ fixation, including nitrate photoassimilation (Bloom et al. 1989) and potentially lipid biosynthesis (Stumpf, Bove, and Goffeau 1963). For example, when wheat (*Triticum aestivum*) seedlings were grown with NH₄⁺, leaf AQ values were 1.21 ± 0.06 . Seedlings grown with NO₃⁻ showed suppressed AQ values of 1.13 ± 0.05 (Smart and Bloom, 2001). Given that both NH₄⁺ and NO₃⁻ were nitrogen sources in both the soil and daily watering in the current study, a major reduction in AQ due to nitrate photoassimilation in poplar leaves in this study is not expected. Thus, the average AQ values determined here for California poplar leaves during PAR (1.25 ± 0.05) and C_i (1.23 ± 0.07) response curves compare well with AQ values (1.21 ± 0.06) determined for wheat leaves supplied with NH₄⁺ (Smart and Bloom 2001). Additional studies with wheat and maize (*Zea mays*) using NH₄⁺ as the nitrogen source also observed similar leaf AQ values in the light (e.g., 1.0–1.3), though some values were less than 1.0 (e.g., 0.8) (Cousins and Bloom 2004). These values are more comparable to the mean AQ value determined here from the leaf temperature response curves (0.87 ± 0.28 , see Table 1). These results support our hypothesis that lipid synthesis in chloroplasts may influence AQ as a function of temperature.

Thus, as shown for nitrate photoassimilation (Bloom et al. 1989), the results are consistent with an increasing

fraction of photosynthetic electron transport (and resulting ATP and NADPH) being allocated to chloroplastic lipid synthesis (e.g., isoprenoids and fatty acids) at high leaf temperature, resulting in significant suppression of AQ (Table 1 and Supporting Information S1: Figure S5). In effect, AQ declines as temperature increases because NOP is more resilient to temperature changes than A_{net} . As temperature increases, ATP and NADPH generated by the light-dependent reactions are increasingly allocated to functions other than CO₂ assimilation, such as lipid synthesis.

Isoprene emission rates can increase to very high leaf temperatures, up to 45°C (Monson et al. 1992). Although isoprene emissions by themselves represent a minor fraction of total ETR (e.g., maximum 1%–4%) (Niinemets et al. 1999; Rodrigues et al. 2020), we suggest that its emissions may be an indicator of overall isoprenoid and fatty acid synthesis rates in chloroplasts, which could be expected to accelerate with temperature, driven by increased ATP/NADPH availability (see Section 4.2). However, quantitative studies on light-dependent fatty acid and isoprenoid synthesis rates as a function of temperature are rare, with most studies quantifying leaf lipid composition profiles rather than synthesis rates. Earlier studies estimated fatty acid synthesis rates using ¹⁴C-acetate labelling of isolated chloroplasts (Heinz and Roughan 1983; Roughan and Ohlrogge, 1996). More recently, ¹³CO₂ labelling studies have shown rapid ¹³C-incorporation into fatty acids (Ohlrogge et al. 2000) and isoprenoids (Karl et al. 2002) within minutes of photosynthesis. When ¹³CO₂ labelling was used to quantify the absolute rate of fatty acid synthesis of Arabidopsis plants, synthesis halted in the dark but proceeded at high rates in the light ($12\text{--}24 \mu\text{g h}^{-1} \text{mg h}^{-1}$). Assuming synthesis of α -linolenic acid (C₁₈H₃₀O₂) and a leaf chlorophyll content of 0.5 mg cm^{-2} , this corresponds to a fatty acid synthesis rate of $0.06\text{--}0.12 \mu\text{mol } \alpha\text{-linolenic acid s}^{-1} \text{m}^{-2}$, requiring a photosynthesis flux of $1.1\text{--}2.2 \mu\text{mol CO}_2 \text{ s}^{-1} \text{m}^{-2}$ (18 mol of CO₂ assimilated/mol of α -linolenic acid synthesized). Presuming a light-saturated A_{net} flux of $7.0 \mu\text{mol CO}_2 \text{ s}^{-1} \text{m}^{-2}$ for *A. thaliana* leaves (Tanaka et al. 2013), this suggests that a substantial fraction (15%–31%) of A_{net} can be allocated to fatty acid synthesis. Studies conducting 2-min pulse-chase ¹⁴CO₂ labelling of *A. thaliana* leaves confirmed that a considerable portion of the assimilated ¹⁴CO₂ ($10.4\% \pm 1.1\%$) can be allocated to lipid synthesis (ethanol-soluble compounds) in the light (Kölling et al. 2015). Thus, studies quantifying total volatile and non-volatile isoprenoid and fatty acid synthesis rates as a function of leaf temperature are needed to quantitatively proceed at high rates proceed at high rates compare lipid synthesis fluxes with A_{net} and NOP in order to evaluate the potential temperature dependency of chloroplast lipid synthesis rates and AQ in the light (see additional discussion on AQ in the Supporting Information S1: Discussion, ‘Plant CO₂/O₂ metabolism and transport and the net assimilatory quotient (AQ)’).

Nonetheless, it is important to note that AQ and RQ (respiration quotient: CO₂ produced/O₂ consumed) values of plant tissues based on gas exchange methods are well known to be difficult to accurately obtain with a high degree of confidence because of the separate analytical techniques required (Scafaro et al. 2017). Systematic errors in either CO₂ flux or O₂ flux measurements will propagate into AQ and RQ values. In studies

of leaf RQ values in the dark, when different methods to measure CO₂ and O₂ fluxes were compared, statistically significant differences were found between them. For example, when three methods to determine leaf dark respiration by fluorophore, O₂ electrode, IRGA and MIMS techniques were compared, substantially different RQ values were obtained (Scafaro et al. 2017). Using leaf dark respiration based on IRGA observations of net CO₂ fluxes in the dark, RQ values equal to 1.0 as well as substantially less and greater than 1.0 could be obtained, depending on the method used to measure O₂ fluxes. Calibration of CO₂ and/or O₂ sensors can improve the accuracy of flux measurements but requires highly accurate and precise gas standards spanning the range in observed concentrations. In our study, we lacked a suite of high-precision CO₂ and O₂ standards and relied on recent factory calibrations for the CO₂ (IRGA) and/or O₂ (CRDS). Our method for AQ determination depends on the slope of the instrument response to small changes (e.g., 0–200 ppm) in O₂ concentrations (the sensitivity). Although we do not have any evidence pointing to this possibility, a slight underestimate of the actual CRDS sensitivity to changes in O₂ concentrations relative to the recent factory calibration would lead to underestimating NOP, and therefore overestimating AQ. Future studies should therefore attempt to address this issue by calibrating CO₂ and O₂ sensors with high-accuracy and high-precision gas standards that span the range of concentrations encountered in dynamic plant enclosures. Calibration of high-precision CO₂ and O₂ sensors has been achieved using high-pressure cylinders of ambient air with known CO₂ and O₂ mole fractions, certified by a specialized laboratory using an LI-6252 for CO₂ (IRGA) and an Oxzilla II (lead fuel cell O₂) (Pickers, 2016). However, regardless of absolute AQ values, our data allows for a relative comparison of AQ changes in response to light, CO₂ and temperature variations.

Given that ETR measured by chlorophyll fluorescence is based on PSII electron flow, and gross rates of oxygen production also reflect PSII activity, a tight correlation is expected between GOP and ETR as leaf temperatures vary in the light. Consistent with this prediction, ETR, determined using the fluorimeter, and δ¹⁸O of O₂ during H₂¹⁸O leaf labelling as a proxy for GOP, both increased to a similar optimal temperature of 35°C before declining at higher temperatures (see Supporting Information S1: Discussion: ‘Pros and cons of the ¹⁸O-labelling method’). This is distinctly higher than the optimal temperature of NOP and A_{net} (31°C). This suggests that the suppression of A_{net} and NOP at high temperatures is mainly due to higher (photo)respiratory CO₂ production/O₂ consumption. This would be consistent with a model where at the optimal temperature for A_{net} and NOP of 31°C in the light, relatively low rates of photorespiration, respiration, lipid biosynthesis (fatty acids and isoprenoids) and CO₂/O₂ recycling occur. In contrast, at the optimal temperature for GOP and ETR (35°C), a reduction in g_s leads to a decrease in gross atmospheric CO₂ uptake, which is partially compensated for by increased re-assimilation of internal CO₂. In effect, there is an increase in CO₂ liberation by photorespiration (due to a decline of RuBisCO specificity and thus an increase in Γ*) and mitochondrial respiration when temperature increases (Voss et al. 2013). This mechanism is illustrated in Figure 7, where the suppression of A_{net} and NOP at 35°C versus 31°C is not due to high temperature stress on

photosynthesis per se, but rather a concurrent change in gross photosynthesis and (photo)respiration, as well as CO₂ and O₂ recycling (Eckert, Jensen, and Gu 2020; Eckert et al. 2021; Garcia et al. 2019). In contrast, temperatures higher than 35°C negatively impacted GOP and ETR, while (photo)respiration and isoprene emissions increased (see T_{opt} values in Table 2 and Figure 6). Due to the concurrent decrease in O₂ production (GOP) and increased O₂ sinks like (photo)respiration, there was a further decline in A_{net} and NOP up to the highest leaf temperature used here (40°C).

4.2 | Isoprene Emission and Its Potential Relationship with NOP and GOP

The response of leaf isoprene emissions to light (PAR), intercellular CO₂ mole fraction (C_i) and leaf temperature was broadly consistent with the common assumption of isoprene energetics models (commonly referred to as Niinemets et al. (1999) model) that isoprene emission relies on available reducing power in chloroplasts (Morfopoulos et al. 2013). Here, we propose that this model could be extended to represent all lipids (isoprenoids and fatty acids) synthesized de novo in chloroplasts. This assumption reflects situations where the demand by the Calvin–Benson cycle for CO₂ assimilation outcompetes other pathways (e.g., the MEP pathway for isoprenoid biosynthesis) for ATP/NADPH (Rodrigues et al. 2020). In fact, CO₂ assimilation and photorespiration are the greatest sinks for ATP/NADPH, and control of lipid synthesis can occur when the effective Michaelis–Menten constant for ATP or/and NADPH is high for the MEP and fatty acid pathways (Rasulov et al. 2016). Thus, one may anticipate that at elevated C_i (e.g., due to elevated atmospheric CO₂), there will be a suppression of isoprene emissions together with a stimulation of A_{net} and NOP due to the increased demand for photosynthetic ATP/NADPH by the Calvin cycle (Morfopoulos et al. 2014; Niinemets et al. 2021; Rasulov et al. 2018), and this is what we observed (Figure 3 and Supporting Information S1: Figure S4). Similarly, at low light, isoprene emissions were barely detectable despite significant NOP and A_{net} fluxes, probably due to limited excess ATP/NADPH. Conversely, under light saturating conditions, further increases in PAR did not significantly enhance A_{net} or NOP, but stimulated increased isoprene emissions, likely due to increased ATP/NADPH availability (Figure 2 and Supporting Information S1: Figure S3) associated with a decline in C_i (Supporting Information S1: Figure S7). Consequently, as predicted from isoprene photosynthesis energetic models and previous experimental observations (Jardine et al. 2016), the fraction of carbon (in % of A_{net} or NOP) emitted as isoprene increased with light intensity (see example Supporting Information S1: Figure S3c).

Also, we observed a progressive increase in isoprene emission with temperature (Figures 4 and 5 and Supporting Information S1: Figures S5 and S6), consistent with previous studies where isoprene emissions increased up to 40°C in many species (Harley, Monson, and Lerdau 1999; Rasulov et al. 2010). As observed here in poplar, ETR is frequently reported to have a higher leaf temperature optimum than A_{net} (Sage and Kubien, 2007). Also, isoprene energetic models predict a temperature optimum for isoprene emission that is strongly influenced by the optimal temperature of ETR and isoprene synthase

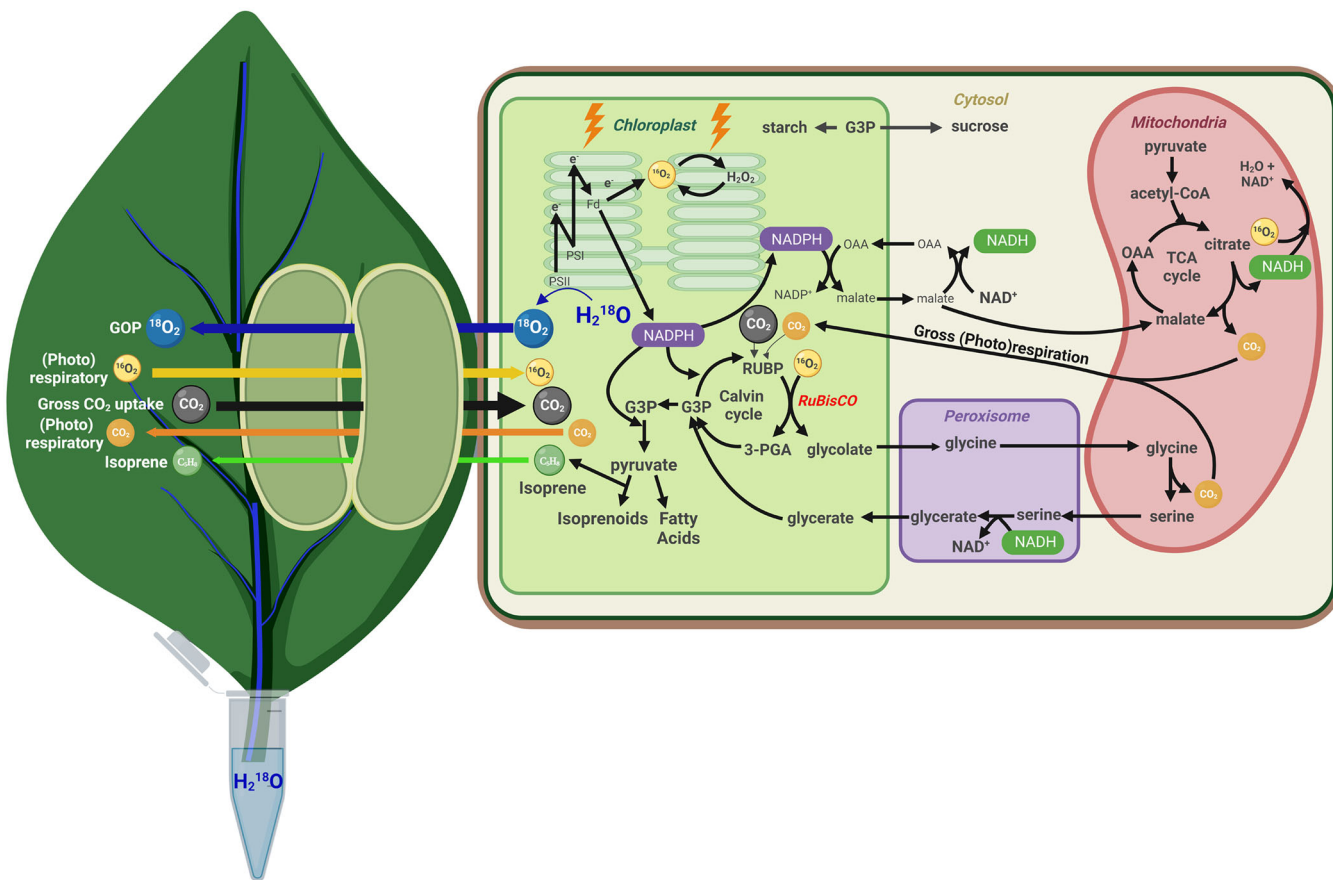


FIGURE 7 | Simplified metabolic model of primary CO_2 and O_2 metabolism at elevated leaf temperatures (e.g., 35°C) in poplar leaves (accelerated metabolism). Elevated temperature leads to a suppression of stomatal conductance (g_s), net oxygen production (NOP) and net atmospheric CO_2 uptake (A_{net}) and a stimulation of photosynthesis, (photo)respiration and internal CO_2/O_2 recycling and isoprenoid synthesis consuming ATP/NADPH. Note the activity of the water–water cycle is depicted as the cycling between O_2 and H_2O_2 .

activity, the latter of which has been reported to be 45°C or higher (Monson et al. 1992; Niinemets et al. 1999; Rasulov et al. 2010). Therefore, at leaf temperatures higher than the ETR and GOP optimum (35°C), the increase in isoprene emissions up to 40°C could be explained by a high temperature optimum for isoprene synthase (e.g., 45°C). However, we note that C_i decreased at leaf temperatures higher than the optimal for g_s (i.e., 33°C) (Supporting Information S1: Figure S7 and Table 2). We thus suggest that in addition to the effect of isoprene synthase thermal optimum, the increase in isoprene emission is also driven by lower ATP/NADPH utilization for carboxylation in the Calvin cycle, resulting from stomatal closure and the decline in C_i . Although O_2 fixation (photorespiration) increasingly consumes photosynthetic ATP/NADPH as temperature increases in the light (Voss et al. 2013), it is believed that lipid biosynthesis also consumes excess ATP/NADPH not utilized by the Calvin and photorespiratory cycles (Rasulov et al. 2009). These processes occur in parallel with other known processes that help relax the chloroplast redox poise at high temperatures including the malate/oxaloacetate shuttle (Selinski and Scheibe 2019) and assimilatory nitrate (Bloom 2015) and sulphate (Abadie and Tcherkez 2019) reduction. Consistent with experimental and modelling studies demonstrating a lack of direct stomatal control over isoprene emissions (Niinemets and Reichstein 2003), we observed isoprene emissions increase with transpiration as a function of temperature despite partial

stomatal closure (Figure 4 and Supporting Information S1: Figure S5). At high leaf temperatures, the continued increase in leaf transpiration can be explained by a dominant effect of increasing leaf-to-atmosphere water vapour concentration gradients (vapour pressure deficit, VPD). Likewise, reduced g_s does not suppress light-dependent isoprene emissions because high production rates quickly generate larger leaf-to-atmosphere isoprene concentration gradients, overcoming stomatal limitations on emissions (Smart and Bloom 2001).

Taken as a whole, our results agree with the availability of ATP/NADPH in the chloroplast being rate-limiting for isoprene synthesis (Rasulov et al. 2009, 2018) and suggest that global carbon-chemistry-climate models that predict isoprene emissions from the terrestrial biosphere using a photosynthesis-based energetics model are valid (Unger et al. 2013). While carbon limitations for isoprene biosynthesis have been generally considered negligible, previous studies using CO_2 -free air demonstrated that light-dependent isoprene emissions can occur at surprisingly high rates. These emissions are light and temperature stimulated, depend on electron transport and are associated with the refixation of (photo)respiratory CO_2 (Garcia et al. 2019). Our observations are consistent with the idea that carbon limitation for isoprene synthesis occurs only at very low C_i (Lantz et al. 2019) and suggest that CO_2 refixation in leaves is a carbon source for isoprene synthesis under photorespiratory

conditions (i.e., high light and temperature) and thus could be a potentially important thermotolerance mechanism (especially if generalizable to light-dependent plastidic lipid synthesis). When photorespiration is high, such as during heat stress, increased lipid synthesis probably contributes to regulating chloroplast redox poise by consuming excess photosynthetic ATP/NADPH. This would in turn help mitigate excessive reactive oxygen species formation and oxidative damage to the photosynthetic machinery and thereby provide resilience to photosynthetic parameters such as maximum carboxylation velocity and membrane stability (Loreto et al. 2001; Loreto & Velikova, 2001). In other words, the present results support the notion that plastidic lipid synthesis plays a role in protecting photosynthesis against damage during high light, heat and drought stress, and therefore plays an important but poorly quantified indirect role in terrestrial carbon cycling under climate extremes (Velikova et al. 2006).

5 | Conclusions and Perspectives

Our study shows that coupling O₂ and isoprene exchange to traditional CO₂/H₂O gas exchange is possible, using CRDS-based oxygen and PTR-MS-based isoprene measurements. This configuration allows a more complete picture of the photosynthetic redox budget via the photosynthetic production of O₂, ETR and isoprene biosynthesis. This opens avenues for useful measurements during photosynthesis, such as the temperature sensitivity of GOP using ¹⁸O-water labelling and the AQ, which appears to be suppressed at high leaf temperature. However, since accurate measurements of both A_{net} and NOP are needed to calculate AQ, great care in calibrating the separate analytical sensors with a suite of high-accuracy standards spanning the observed concentration range is needed. Also, our findings may help resolve some confusion in the literature regarding whether isoprene emissions, and perhaps lipid synthesis in chloroplasts in general, are directly linked to net photosynthesis. In agreement with numerous previous studies, we found that isoprene emission can be uncoupled from A_{net}, that is, at low C_i and high temperature (Figures 3 and 4 and Supporting Information S1: Figures S4 and S5), and thus it is unlikely that lipid biosynthesis in chloroplasts strictly depends on photosynthesis rate or carbon provision by photosynthates. Therefore, our results suggest that (i) isoprene synthesis (and potentially lipid synthesis in general) in chloroplasts is related to electron generation by photolysis and thus probably via excess photosynthetic ATP/NADPH (not consumed by the Calvin cycle, the photorespiratory cycle and other pathways acting in parallel like the malate/oxaloacetate shuttle), and (ii) is carbon-limited only when gross photosynthesis declines considerably. We nevertheless recognize that dual isotopic labelling with ¹³CO₂ and ¹⁸O-water together with total isoprenoid and fatty acid synthesis rates would be useful to ascertain this and quantify precisely the temperature dependencies between ¹³C-lipid appearance and ¹⁸O₂ evolution. This will be addressed in another study.

Acknowledgements

We kindly thank Bryan Taylor at Lawrence Berkeley National Laboratory for the technical support. This material is based upon work

supported by the US Department of Energy (DOE), Office of Science, Office of Biological and Environmental Research (BER), Biological System Science Division (BSSD), Early Career Research Programme under Award Number FP00007421 to K. Jardine and at the Lawrence Berkeley National Laboratory. Additional DOE support was provided by the Next-Generation Ecosystem Experiments-Tropics (NGEE-Tropics) through Contract No. DE-AC02-05CH11231 as part of DOE's Terrestrial Ecosystem Science Programme.

Conflicts of Interest

The authors declare no conflicts of interest.

Data Availability Statement

The data that supports the findings of this study are available in the Supporting Information of this article.

References

- Abadie, C., and G. Tcherkez. 2019. "Plant Sulphur Metabolism Is Stimulated by Photorespiration." *Communications Biology* 2, no. 1: 379.
- Allahverdiyeva, Y., J. Isojärvi, P. Zhang, and E.-M. Aro. 2015. "Cyanobacterial Oxygenic Photosynthesis Is Protected by Flavodiiron Proteins." *Life* 5, no. 1: 716–743.
- Bloom, A. J. 2015. "The Increasing Importance of Distinguishing Among Plant Nitrogen Sources." *Current Opinion in Plant Biology* 25: 10–16.
- Bloom, A. J., R. M. Caldwell, J. Finazzo, R. L. Warner, and J. Weissbart. 1989. "Oxygen and Carbon Dioxide Fluxes From Barley Shoots Depend on Nitrate Assimilation." *Plant Physiology* 91, no. 1: 352–356.
- Bloom, A. J., D. R. Smart, D. T. Nguyen, and P. S. Searles. 2002. "Nitrogen Assimilation and Growth of Wheat Under Elevated Carbon Dioxide." *Proceedings of the National Academy of Sciences of the United States of America* 99, no. 3: 1730–1735.
- Bolton, P., and J. L. Harwood. 1978. "Fatty Acid Synthesis by Slices From Developing Leaves." *Planta* 138: 223–228.
- Canvin, D. T., J. A. Berry, M. R. Badger, H. Fock, and C. B. Osmond. 1980. "Oxygen Exchange in Leaves in the Light." *Plant Physiology* 66, no. 2: 302–307.
- Cen, Y.-P., D. H. Turpin, and D. B. Layzell. 2001. "Whole-Plant Gas Exchange and Reductive Biosynthesis in White Lupin." *Plant Physiology* 126, no. 4: 1555–1565.
- Chen, J., J. J. Burke, Z. Xin, C. Xu, and J. Velten. 2006. "Characterization of the Arabidopsis Thermosensitive Mutant atts02 Reveals an Important Role for Galactolipids in Thermotolerance." *Plant, Cell & Environment* 29, no. 7: 1437–1448.
- Cousins, A., and A. Bloom. 2003. "Influence of Elevated CO₂ and Nitrogen Nutrition on Photosynthesis and Nitrate Photo-Assimilation in Maize (*Zea mays* L.)." *Plant, Cell & Environment* 26, no. 9: 1525–1530.
- Cousins, A., and A. Bloom. 2004. "Oxygen Consumption During Leaf Nitrate Assimilation in a C3 and C4 Plant: The Role of Mitochondrial Respiration." *Plant, Cell & Environment* 27, no. 12: 1537–1545.
- Earl, H. J., and M. Tollenaar. 1998. "Relationship Between Thylakoid Electron Transport and Photosynthetic CO₂ Uptake in Leaves of Three Maize (*Zea mays* L.) Hybrids." *Photosynthesis Research* 58: 245–257.
- Eckert, D., A. M. Jensen, and L. Gu. 2020. "The Maximum Carboxylation Rate of Rubisco Affects CO₂ Refixation in Temperate Broadleaved Forest Trees." *Plant Physiology and Biochemistry* 155: 330–337.
- Eckert, D., H. J. Martens, L. Gu, and A. M. Jensen. 2021. "CO₂ Refixation Is Higher in Leaves of Woody Species With High Mesophyll and Stomatal Resistances to CO₂ Diffusion." *Tree Physiology* 41, no. 8: 1450–1461.

- Eisenreich, W., A. Bacher, D. Arigoni, and F. Rohdich. 2004. "Biosynthesis of Isoprenoids via the Non-Mevalonate Pathway." *Cellular and Molecular Life Sciences* 61: 1401–1426.
- Funk, J., J. Mak, and M. Lerdau. 2004. "Stress-Induced Changes in Carbon Sources for Isoprene Production in *Populus deltoides*." *Plant, Cell & Environment* 27, no. 6: 747–755.
- Garcia, S., K. Jardine, V. Souza, R. Souza, S. Duvoisin Junior, and J. Gonçalves. 2019. "Reassimilation of Leaf Internal CO₂ Contributes to Isoprene Emission in the Neotropical Species *Inga edulis* Mart." *Forests* 10, no. 6: 472.
- Gauthier, P. P. G., M. O. Battle, K. L. Griffin, and M. L. Bender. 2018. "Measurement of Gross Photosynthesis, Respiration in the Light, and Mesophyll Conductance Using H₂¹⁸O Labeling." *Plant Physiology* 177, no. 1: 62–74.
- Gimenez, B. O., K. J. Jardine, N. Higuchi, et al. 2019. "Species-Specific Shifts in Diurnal Sap Velocity Dynamics and Hysteretic Behavior of Ecophysiological Variables During the 2015–2016 El Niño Event in the Amazon Forest." *Frontiers in Plant Science* 10: 830.
- Harley, P. C., R. K. Monson, and M. T. Lerdau. 1999. "Ecological and Evolutionary Aspects of Isoprene Emission From Plants." *Oecologia* 118: 109–123.
- Haupt-Herting, S. 2002. "Oxygen Exchange in Relation to Carbon Assimilation in Water-Stressed Leaves During Photosynthesis." *Annals of Botany* 89, no. 7: 851–859.
- Heinz, E., and P. G. Roughan. 1983. "Similarities and Differences in Lipid Metabolism of Chloroplasts Isolated From 18:3 and 16:3 Plants." *Plant Physiology* 72, no. 2: 273–279.
- Hikosaka, K., K. Ishikawa, A. Borjigidai, O. Muller, and Y. Onoda. 2006. "Temperature Acclimation of Photosynthesis: Mechanisms Involved in the Changes in Temperature Dependence of Photosynthetic Rate." *Journal of Experimental Botany* 57, no. 2: 291–302.
- Jardine, K., J. Chambers, E. G. Alves, et al. 2014. "Dynamic Balancing of Isoprene Carbon Sources Reflects Photosynthetic and Photorespiratory Responses to Temperature Stress." *Plant Physiology* 166, no. 4: 2051–2064.
- Jardine, K. J., A. B. Jardine, V. F. Souza, et al. 2016. "Methanol and Isoprene Emissions From the Fast Growing Tropical Pioneer Species *Vismia guianensis* (Aubl.) Pers. (Hypericaceae) in the Central Amazon Forest." *Atmospheric Chemistry and Physics* 16, no. 10: 6441–6452.
- Jardine, K. J., E. D. Sommer, S. R. Saleska, T. E. Huxman, P. C. Harley, and L. Abrell. 2010. "Gas Phase Measurements of Pyruvic Acid and Its Volatile Metabolites." *Environmental Science & Technology* 44, no. 7: 2454–2460.
- Jardine, K. J., R. F. Zorzanelli, B. O. Gimenez, et al. 2020. "Leaf Isoprene and Monoterpene Emission Distribution Across Hyperdominant Tree Genera in the Amazon Basin." *Phytochemistry* 175: 112366.
- Kang, H.-X., X.-G. Zhu, W. Yamori, and Y.-H. Tang. 2020. "Concurrent Increases in Leaf Temperature With Light Accelerate Photosynthetic Induction in Tropical Tree Seedlings." *Frontiers in Plant Science* 11: 569407.
- Karl, T., R. Fall, T. Rosenstiel, et al. 2002. "On-Line Analysis of the ¹³CO₂ Labeling of Leaf Isoprene Suggests Multiple Subcellular Origins of Isoprene Precursors." *Planta* 215: 894–905.
- Kim-Hak, D., J. Hoffnagle, D. Lynch, and M. Johnson. 2018. "High Precision Continuous and Real-Time Measurement of Oxygen Using Cavity Ring-Down Spectroscopy for Photosynthetic Light-Response Studies." Paper presented at the AGU Fall Meeting Abstracts, Washington, D.C., USA, December 13, 2018.
- Kölling, K., M. Thalmann, A. Müller, C. Jenny, and S. C. Zeeman. 2015. "Carbon Partitioning in *Arabidopsis thaliana* Is a Dynamic Process Controlled by the Plants Metabolic Status and Its Circadian Clock." *Plant, Cell & Environment* 38, no. 10: 1965–1979.
- Kreuzwieser, J., M. Graus, A. Wisthaler, A. Hansel, H. Rennenberg, and J. P. Schnitzler. 2002. "Xylem-Transported Glucose as an Additional Carbon Source for Leaf Isoprene Formation in *Quercus robur*." *New Phytologist* 156, no. 2: 171–178.
- Kull, O. 2002. "Acclimation of Photosynthesis in Canopies: Models and Limitations." *Oecologia* 133: 267–279.
- Laisk, A., V. Oja, B. Rasulov, H. Rämme. 2002. "A Computer-Operated Routine of Gas Exchange and Optical Measurements to Diagnose Photosynthetic Apparatus in Leaves." *Plant, Cell & Environment* 25, no. 7: 923–943.
- Lantz, A. T., C. Solomon, L. Gog, et al. 2019. "Isoprene Suppression by CO₂ Is Not Due to Triose Phosphate Utilization (TPU) Limitation." *Frontiers in Forests and Global Change* 2: 8.
- LI-COR. 2023. "Leaf-Level O₂ and CO₂ Measurements With the LI-6800 and Picarro G2207-i: Application Note." <https://www.licor.com/documents/6dmmzntry4uey6un6m6hfwpx7t8ssp5>.
- Long, S. 1991. "Modification of the Response of Photosynthetic Productivity to Rising Temperature by Atmospheric CO₂ Concentrations: Has Its Importance Been Underestimated?" *Plant, Cell & Environment* 14, no. 8: 729–739.
- Loreto, F., M. Mannozi, C. Maris, P. Nascetti, F. Ferranti, and S. Pasqualini. 2001. "Ozone Quenching Properties of Isoprene and Its Antioxidant Role in Leaves." *Plant Physiology* 126, no. 3: 993–1000.
- Loreto, F., and T. D. Sharkey. 1990. "A Gas-Exchange Study of Photosynthesis and Isoprene Emission in *Quercus rubra* L." *Planta* 182, no. 4: 523–531.
- Loreto, F., and V. Velikova. 2001. "Isoprene Produced by Leaves Protects the Photosynthetic Apparatus Against Ozone Damage, Quenches Ozone Products, and Reduces Lipid Peroxidation of Cellular Membranes." *Plant Physiology* 127, no. 4: 1781–1787.
- Ma, Q., M. H. Behboudian, N. C. Turner, and J. A. Palta. 2001. "Gas Exchange by Pods and Subtending Leaves and Internal Recycling of CO₂ by Pods of Chickpea (*Cicer arietinum* L.) Subjected to Water Deficits." *Journal of Experimental Botany* 52, no. 354: 123–131.
- Monson, R. K., C. H. Jaeger, W. W. Adams, E. M. Driggers, G. M. Silver, and R. Fall. 1992. "Relationships Among Isoprene Emission Rate, Photosynthesis, and Isoprene Synthase Activity as Influenced by Temperature." *Plant Physiology* 98, no. 3: 1175–1180.
- Monson, R. K., B. Winkler, T. N. Rosenstiel, et al. 2020. "High Productivity in Hybrid-Poplar Plantations Without Isoprene Emission to the Atmosphere." *Proceedings of the National Academy of Sciences of the United States of America* 117, no. 3: 1596–1605.
- Morfopoulos, C., I. C. Prentice, T. F. Keenan, et al. 2013. "A Unifying Conceptual Model for the Environmental Responses of Isoprene Emissions From Plants." *Annals of Botany* 112, no. 7: 1223–1238.
- Morfopoulos, C., D. Sperlich, J. Peñuelas, et al. 2014. "A Model of Plant Isoprene Emission Based on Available Reducing Power Captures Responses to Atmospheric CO₂." *New Phytologist* 203, no. 1: 125–139.
- Niemiec, S. S., G. R. Ahrens, S. Willits, and D. E. Hibbs. 1995. *Hardwoods of the Pacific Northwest*. Corvallis, OR: Oregon State University.
- Niinemets, Ü., B. Rasulov, and E. Talts. 2021. "CO₂-Responsiveness of Leaf Isoprene Emission: Why Do Species Differ." *Plant, Cell & Environment* 44, no. 9: 3049–3063.
- Niinemets, Ü., and M. Reichstein. 2003. "Controls on the Emission of Plant Volatiles Through Stomata: Differential Sensitivity of Emission Rates to Stomatal Closure Explained." *Journal of Geophysical Research: Atmospheres* 108, no. D7: 4208.
- Niinemets, Ü., J. D. Tenhunen, P. C. Harley, and R. Steinbrecher. 1999. "A Model of Isoprene Emission Based on Energetic Requirements for Isoprene Synthesis and Leaf Photosynthetic Properties for Liquidambar and Quercus." *Plant, Cell & Environment* 22, no. 11: 1319–1335.

- Noctor, G., and C. H. Foyer. 1998. "A Re-Evaluation of the ATP: NADPH Budget During C3 Photosynthesis: A Contribution From Nitrate Assimilation and Its Associated Respiratory Activity." *Journal of Experimental Botany* 49, no. 329: 1895–1908.
- Ohlrogge, J., M. Pollard, X. Bao, et al. 2000. "Fatty Acid Synthesis: From CO₂ to Functional Genomics." *Biochemical Society Transactions* 28, no. 6: 567–574.
- Pickers, P. 2016. *New Applications of Continuous Atmospheric O₂ Measurements: Meridional Transects Across the Atlantic Ocean, and Improved Quantification of Fossil Fuel-Derived CO₂*. Norwich, UK: University of East Anglia.
- Rasulov, B., I. Bichele, A. Laisk, and Ü. Niinemets. 2014. "Competition Between Isoprene Emission and Pigment Synthesis During Leaf Development in Aspen." *Plant, Cell & Environment* 37, no. 3: 724–741.
- Rasulov, B., K. Hüve, I. Bichele, A. Laisk, and Ü. Niinemets. 2010. "Temperature Response of Isoprene Emission In Vivo Reflects a Combined Effect of Substrate Limitations and Isoprene Synthase Activity: A Kinetic Analysis." *Plant Physiology* 154, no. 3: 1558–1570.
- Rasulov, B., K. Hüve, M. Vålbe, A. Laisk, and Ü. Niinemets. 2009. "Evidence That Light, Carbon Dioxide, and Oxygen Dependencies of Leaf Isoprene Emission Are Driven by Energy Status in Hybrid Aspen." *Plant Physiology* 151, no. 1: 448–460.
- Rasulov, B., E. Talts, I. Bichele, and Ü. Niinemets. 2018. "Evidence That Isoprene Emission Is Not Limited by Cytosolic Metabolites. Exogenous Malate Does Not Invert the Reverse Sensitivity of Isoprene Emission to High [CO₂]." *Plant Physiology* 176, no. 2: 1573–1586.
- Rasulov, B., E. Talts, and Ü. Niinemets. 2016. "Spectacular Oscillations in Plant Isoprene Emission Under Transient Conditions Explain the Enigmatic CO₂ Response." *Plant Physiology* 172: 2275–2285.
- Rodrigues, T. B., C. R. Baker, A. P. Walker, et al. 2020. "Stimulation of Isoprene Emissions and Electron Transport Rates as Key Mechanisms of Thermal Tolerance in the Tropical Species *Vismia guianensis*." *Global Change Biology* 26, no. 10: 5928–5941.
- Roughan, P. G., and J. B. Ohlrogge. 1996. "Evidence That Isolated Chloroplasts Contain an Integrated Lipid-Synthesizing Assembly That Channels Acetate Into Long-Chain Fatty Acids." *Plant Physiology* 110, no. 4: 1239–1247.
- Sage, R. F., and D. S. Kubien. 2007. "The Temperature Response of C3 and C4 Photosynthesis." *Plant, Cell & Environment* 30, no. 9: 1086–1106.
- Scafaro, A. P., A. C. A. Negrini, B. O'Leary, et al. 2017. "The Combination of Gas-Phase Fluorophore Technology and Automation to Enable High-Throughput Analysis of Plant Respiration." *Plant Methods* 13, no. 1: 16.
- Searles, P. S., and A. J. Bloom. 2003. "Nitrate Photo-Assimilation in Tomato Leaves Under Short-Term Exposure to Elevated Carbon Dioxide and Low Oxygen." *Plant, Cell & Environment* 26, no. 8: 1247–1255.
- Selinski, J., and R. Scheibe. 2019. "Malate Valves: Old Shuttles With New Perspectives." *Plant Biology* 21: 21–30.
- Sharkey, T. D. 1990. "Feedback Limitation of Photosynthesis and the Physiological Role of Ribulose Bisphosphate Carboxylase Carbamylation." *Botanical Magazine Tokyo Special Issue* 2: 87–105.
- Sharkey, T. D., and S. Yeh. 2001. "Isoprene Emission From Plants." *Annual Review of Plant Physiology and Plant Molecular Biology* 52, no. 1: 407–436.
- Shiva, S., T. Samarakoon, K. A. Lowe, et al. 2020. "Leaf Lipid Alterations in Response to Heat Stress of *Arabidopsis thaliana*." *Plants* 9, no. 7: 845.
- Smart, D. R., and A. J. Bloom. 2001. "Wheat Leaves Emit Nitrous Oxide During Nitrate Assimilation." *Proceedings of the National Academy of Sciences of the United States of America* 98, no. 14: 7875–7878.
- Stumpf, P. K., J. M. Bové, and A. Goffeau. 1963. "Fat Metabolism in Higher Plants XX. Relation of Fatty Acid Synthesis and Photo-phosphorylation in Lettuce Chloroplasts." *Biochimica et Biophysica Acta* 70: 260–270.
- Tanaka, Y., S. S. Sugano, T. Shimada, and I. Hara-Nishimura. 2013. "Enhancement of Leaf Photosynthetic Capacity Through Increased Stomatal Density in Arabidopsis." *New Phytologist* 198, no. 3: 757–764.
- Tcherkez, G., P. Gauthier, T. N. Buckley, et al. 2017. "Leaf Day Respiration: Low CO₂ Flux but High Significance for Metabolism and Carbon Balance." *New Phytologist* 216, no. 4: 986–1001.
- Tcherkez, G., and A. M. Limami. 2019. "Net Photosynthetic CO₂ Assimilation: More Than Just CO₂ and O₂ Reduction Cycles." *New Phytologist* 223, no. 2: 520–529.
- Tovar-Méndez, A., J. A. Miernyk, and D. D. Randall. 2003. "Regulation of Pyruvate Dehydrogenase Complex Activity in Plant Cells." *European Journal of Biochemistry* 270, no. 6: 1043–1049.
- Unger, N., K. Harper, Y. Zheng, et al. 2013. "Photosynthesis-Dependent Isoprene Emission From Leaf to Planet in a Global Carbon-Chemistry-Climate Model." *Atmospheric Chemistry and Physics* 13, no. 20: 10243–10269.
- Usda, N. 2024. "The PLANTS Database." <http://plants.usda.gov>.
- Velikova, V., F. Loreto, T. Tsonev, F. Brilli, and A. Edreva. 2006. "Isoprene Prevents the Negative Consequences of High Temperature Stress in *Platanus orientalis* Leaves." *Functional Plant Biology* 33, no. 10: 931–940.
- Voss, I., B. Sunil, R. Scheibe, and A. S. Raghavendra. 2013. "Emerging Concept for the Role of Photorespiration as an Important Part of Abiotic Stress Response." *Plant Biology* 15, no. 4: 713–722.
- Wahid, A., S. Gelani, M. Ashraf, and M. Foolad. 2007. "Heat Tolerance in Plants: An Overview." *Environmental and Experimental Botany* 61, no. 3: 199–223.
- Walker, B. J., A. VanLoocke, C. J. Bernacchi, and D. R. Ort. 2016. "The Costs of Photorespiration to Food Production Now and in the Future." *Annual Review of Plant Biology* 67: 107–129.
- White, R. H., S. Anderson, J. F. Booth, et al. 2023. "The Unprecedented Pacific Northwest Heatwave of June 2021." *Nature Communications* 14, no. 1: 727.
- Wolfe, D. W., R. M. Gifford, D. Hilbert, and Y. Luo. 1998. "Integration of Photosynthetic Acclimation to CO₂ at the Whole-Plant Level." *Global Change Biology* 4, no. 8: 879–893.
- WRCC. 1941–2012. "Period of Record General Climate Summary." The Poplars, Oregon—Temperature. <https://wrcc.dri.edu/cgi-bin/cliMAIN.pl?or8420>.
- Yang, J. T., A. L. Preiser, Z. Li, S. E. Weise, and T. D. Sharkey. 2016. "Triose Phosphate Use Limitation of Photosynthesis: Short-Term and Long-Term Effects." *Planta* 243, no. 3: 687–698. <https://doi.org/10.1007/s00425-015-2436-8>.

Supporting Information

Additional supporting information can be found online in the Supporting Information section.